GLOBAL BIOGEOCHEMICAL CYCLES, VOL. 27, 1–20, doi:10.1002/gbc.20029, 2013

Revisiting "nutrient trapping" in global coupled biogeochemical ocean circulation models

H. Dietze[1] and U. Loeptien[1,2]

Received 1 August 2012; revised 27 December 2012; accepted 13 February 2013.

[1] We analyze an extensive set of global coupled biogeochemical ocean circulation models. The focus is on the equatorial Pacific. In all simulations, which are consistent with observed standing stocks of relevant biogeochemical species at the surface, we find spuriously enhanced (reduced) macronutrient (oxygen) concentrations in the deep eastern equatorial Pacific. This modeling problem, apparently endemic to global coupled biogeochemical ocean circulation models, was coined "nutrient trapping" by Najjar et al. (1992). In contrast to Aumont et al. (1999), we argue that "nutrient trapping" is still a persistent problem, even in eddy-permitting models and, further, that the scale of the problem retards model projections of nitrogen cycling. In line with previous work, our results indicate that a deficient circulation is at the core of the problem rather than an admittedly poor quantitative understanding of biogeochemical cycles. More specifically, we present indications that "nutrient trapping" in models is a result of a spuriously damped Equatorial Intermediate (zonal) Current System and Equatorial Deep Jets—phenomenon which await a comprehensive understanding and have, to date, not been successfully simulated.

Citation: Dietze, H., and U. Loeptien (2013), Revisiting "nutrient trapping" in global coupled biogeochemical ocean circulation models, *Global Biogeochem. Cycles*, *27*, doi:10.1002/gbc.20029.

1. Introduction

[2] The eastern equatorial Pacific, home to exceptionally strong air-sea exchange of heat, water and carbon is a key region determining global climate variability. Consequently, the region puts our understanding of the interactions between atmosphere, ocean, and pelagic biogeochemical cycling, as expressed in numerical models, to the test. The major and most notorious problems associated with the atmospheric and oceanic model components are a spurious double-split Intertropical Convergence Zone (ITCZ), and a deficient representation of relatively low sea surface temperatures within a zonal band stretching from the western coast of South America far westward into the basin, the so-called "cold-tongue" (Figure 1).

[3] Given the especially tight coupling between the atmosphere and the ocean in the region, it is straightforward to seek a common cause of these notorious problems. On the other hand, it is just that tight (and nonlinear) coupling in combination with high uncertainties in flux estimates (e.g., Figure 2) which makes it difficult to even go the first step and identify which of the model components is most deficient. To complicate things further, the region is one example of few where biotic feedbacks on climate dynamics are significant because the solar radiation absorbed by phytoplankton pigments drives considerable heating of the surface ocean thereby modulating the coupling between ocean and atmosphere [e.g., *Loeptien et al*., 2009].

[4] Various attempts to identify deficiencies in the atmospheric and oceanic modules are documented in the literature. Among them are studies focusing on (1) cloud parameterizations in the atmosphere, (2) the effect of coarse spacial resolution of the ocean which fails to resolve tropical instability waves and topographic effects on the equatorial current system, (3) numerical subtleness associated with ocean-atmosphere couplers, and (4) the neglected effect of phytoplankton on the heat budget. Even so, the problems (double-split ITCZ and sea surface temperature bias) are apparently still exigent because they persist in all the IPCC AR4 models that were not flux-corrected.

[5] To this end, it seems remarkable that, of all model deficiencies in the region, the problem of spuriously enhanced nutrient concentrations in the deep eastern equatorial Pacific was apparently solved in isolation. This problem of coupled biogeochemical ocean circulation models was dubbed "nutrient trapping" by *Najjar et al.* [1992] and, supposedly, was solved by *Aumont et al.* [1999] who related it to a sluggish representation of the equatorial undercurrent in coarse resolution models. In contrast to *Aumont et al.* [1999], we argue in section 1.1 that "nutrient trapping" is also a persistent problem still exigent insofar as it retards simulations of dissolved oxygen and, in turn, of denitrification.

[1]GEOMAR, Helmholtz Centre for Ocean Research Kiel, Kiel, Germany.
[2] Department of Oceanography, Swedish Meteorological and Hydrological Institute (SMHI), Norrköping, Sweden.

Corresponding author: H. Dietze, GEOMAR, Helmholtz Centre for Ocean Research Kiel, Düsternbrooker Weg 20, D-24105 Kiel, Germany. (hdietze@geomar.de)

0886-6236/13/10.1002/gbc.20029

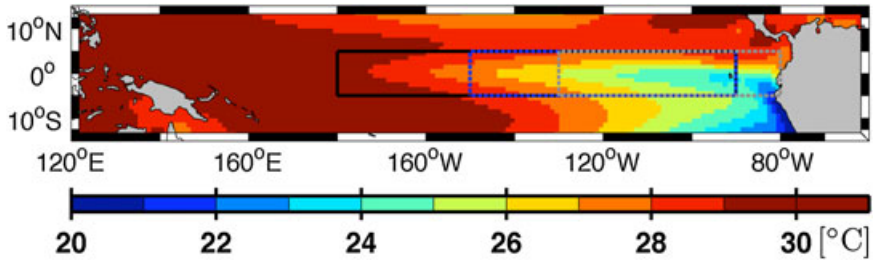

Figure 1. Climatological, annual mean sea surface temperature from *Reynolds et al.* [2002]. Locations of this and related studies are superposed: the black line comprises the "upwelling box" of *Wyrtki* [1981]. The gray, dashed line comprises the "nutrient trapping box" of *Maier-Reimer* [1993], *Najjar et al.* [1992], *Aumont et al.* [1999], and this study. The blue line comprises the "heat flux box" (Ninõ-3 region) used in, e.g., *Zhang and McPhaden* [2010].

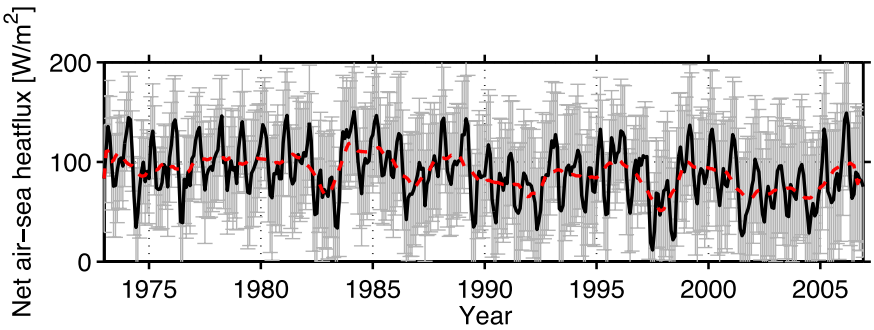

Figure 2. Net air-sea heatflux estimate from the NOCS Surface Flux Dataset v2.0 [*Berry and Kent*, 2011] averaged over the Ninõ-3 region (150°W–90°W, 5°S–9°S). The black and red lines denote monthly mean fluxes and a running mean averaged over 12 months, respectively. The gray lines show uncertainties of monthly mean fluxes.

[6] The remainder of the paper explores the sensitivity of the "nutrient trapping" problem by examining a suite of coupled ocean circulation ecosystem models. The suite is, compared to previous studies, relatively exhaustive. It comprises, e.g., varying horizontal resolutions down to eddy-permitting, differing vertical resolutions, differing atmospheric forcing as well as a wide range of ecosystem models. The latter differ with respect to both their prognostic variables and their associated parameters. A description of the simulations is summarized in section 2 and elaborated on in the Appendix A. Section 2.2 explains how we measure "nutrient trapping" in our simulations. Model results are presented, discussed, and summarized in sections 3, 4, and 5, respectively.

1.1. "Nutrient Trapping"—A Persistent Problem

[7] Concerns about anthropogenic radiative forcing triggered the development of global coupled ocean-carbon models with a realistic ocean topography and a rough representation of biotic effects on carbon cycles [*Najjar et al.*, 1992; *Maier-Reimer*, 1993]. These models were in reasonable agreement with observations of phosphate in general, yet they shared a common flaw in the eastern equatorial Pacific: a pronounced, up to 50%, high bias in subsurface phosphate concentrations. This model deficiency is generally referred to as "nutrient trapping," a term coined by *Najjar et al.* [1992] to explain (deficient) model dynamics in that zone, which feeds the equatorial upwelling. Note that (as pointed out by *Najjar et al.* [1992]) "nutrient trapping" cannot explain spuriously enhanced nutrient concentrations deeper in the thermocline. Insofar the general usage of the term is inexact. Here we comply with the majority in order to avoid to invent another terminology. More specifically we use "nutrient trapping" to name spuriously enhanced water column nutrient inventories below the equatorial undercurrent.

[8] Sensitivity studies suggested that the problem was not related to a deficient parameterization of sinking particulate organic matter (POM). For example, *Maier-Reimer* [1993] found that the scale of the problem was insensitive toward changes of the parameterization of the POM remineralization. In his model framework, "nutrient trapping" could merely be shifted in the vertical and distributed over a larger volume. He speculated that the problem is associated with flaws in his physical circulation model, "... perhaps as a consequence of the coarse vertical resolution of the models."

[9] *Najjar et al.* [1992], on the other hand, showed that a fundamentally different understanding of the biogeochemical cycling and associated export pathways of organic matter to depth resulted in a model, apparently consistent with observations. Their concept includes an additional explicit representation of dissolved organic matter (DOM) which does not, in contrast to particulate organic matter, sink. This decouples remineralization of organic material (and associated buildup of inorganic nutrients and oxygen deficit) at depth from local photosynthetic production above—if the

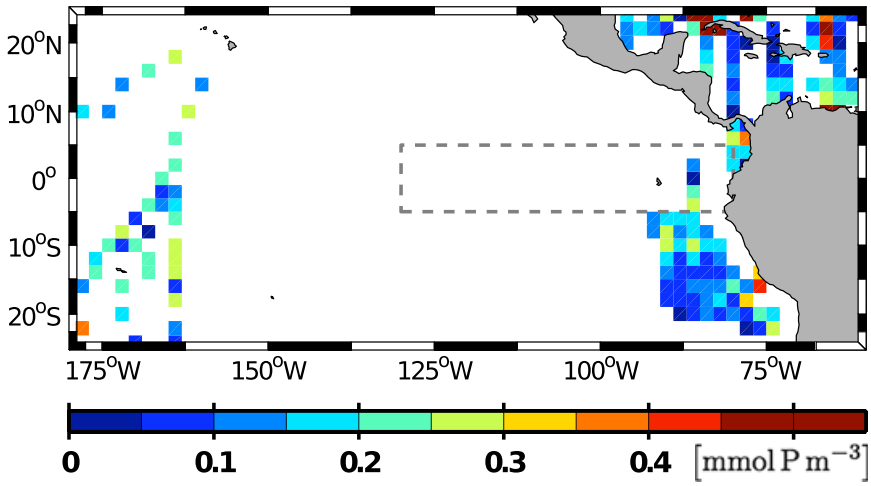

Figure 3. Observed dissolved organic phosphorous surface concentrations from the Global Open Ocean DOP database [*Karl and Björkman*, 2002]. The dashed gray line denotes the "nutrient trapping" region. The data are binned into 2° × 2° latitude-longitude boxes. Missing data are denoted by white areas.

time scale of DOM decay is long enough (Appendix B) to ensure horizontal export out of the equatorial region.

[10] After it became apparent that the *Najjar et al.* [1992] fix to the problem must be accompanied with a simulated DOM pool, way higher than can be inferred from (admittedly sparse, compare Figure 3) observations, various studies presented evidence that the problem lies in the simulated ocean circulation [*Matear and Holloway*, 1995; *Anderson and Sarmiento*, 1995; *Oschlies*, 2000].

[11] To date, and given that an adequate numerical algorithm is applied [*Oschlies*, 2000], *Aumont et al.* [1999] summarize the state-of-the-art. By increasing the meridional resolution to 0.5° they model a stronger, more realistic, equatorial undercurrent that feeds the upwelling in the eastern equatorial Pacific with low-nutrient water from the western basin. This, in turn, effects simulated subsurface nutrient concentrations which exceed observed values by less than 15%. Because their model does not include a DOM pool, this indeed is apparently the "the ocean circulation solution" to the "nutrient trapping" problem.

[12] However, two open questions remain. First, we argue in section 1.1.1 that the role of particulate organic matter (POM) is unclear in the "ocean circulation solution" of *Aumont et al.* [1999]. Their POM compartment could be unrealistically high and might have taken over the role of the unrealistically high DOM concentrations that are needed in other models. Second, we argue (in section 1.1.2) that even a bias as low as 10% in simulated phosphate would not be a real solution to the "nutrient trapping" problem, because the associated oxygen bias renders vast areas of the Pacific suboxic thereby retarding simulations of denitrification.

1.1.1. Decoupling Role of DOM and POM in Models

[13] The definition of DOM in global coupled biogeochemical ocean circulation models is ambiguous. The operational definition is based on size, or on the ability to pass a filter of certain mesh size. Most models do not care about size and the model-relevant trait is that DOM is considered to be dissolved, or at least "too small to sink." The introduction of DOM influences model solutions in that it decouples local primary production from local export of organic material to depth because divergent horizontal surface currents tend to transport DOM away from its production site. After its decay, remineralized nutrients are prone to drive photosynthetic production and associated export elsewhere, i.e., downstream. Because primary production is highly correlated with diffusive or advective nutrient supply to the euphotic zone it is admissible to conclude that the functional role of DOM in a biogeochemical model, is to decouple local export production from the local supply of inorganic nutrients to the euphotic zone. It is hard to overrate the impact of DOM dynamics in models given that a biogeochemical module does, mechanistically, merely two things: first, it redistributes inorganic nutrients supplied to the surface vertically (mimicking sinking and decaying organic matter). Second, it leaves the remainder of the supplied nutrients at the surface (be it in inorganic or organic form) which, as explained above, decouples local nutrient supply from local export. Hence, it is not surprising why—although neither its production nor its decomposition are comprehensively understood—DOM is generally explicitly simulated, and why models show such a high sensitivity toward the exact formulation of DOM dynamics (as reported by, e.g., *Kwon and Primeau* [2006]). Counterintuitive, on the other hand, is that standing surface stocks of plankton and detritus—compartments generally attributed to POM rather than to DOM—are similar to DOM. Bluntly put, POM is identical to DOM because surface currents do not differentiate between sinking and non-sinking organic matter, i.e., both are flushed downstream. Hence, the extent of decoupling between local nutrient supply and local export is effected by the divergent horizontal transport of *total* nutrients in the euphotic zone, including all organic and inorganic forms.

[14] *Aumont et al.* [1999] claim to reduce the "nutrient trapping" without introducing DOM. At the same time they included a spurious POM compartment. Spurious—because in their framework POM is not remineralized under low oxygen concentrations, i.e., it accumulates. It cannot be ruled out that their POM accumulates up to unrealistically high levels thereby causing an unrealistically high (organic) nutrient transport out of the "nutrient trapping" region, or in other words, the POM compartment of *Aumont et al.* [1999],

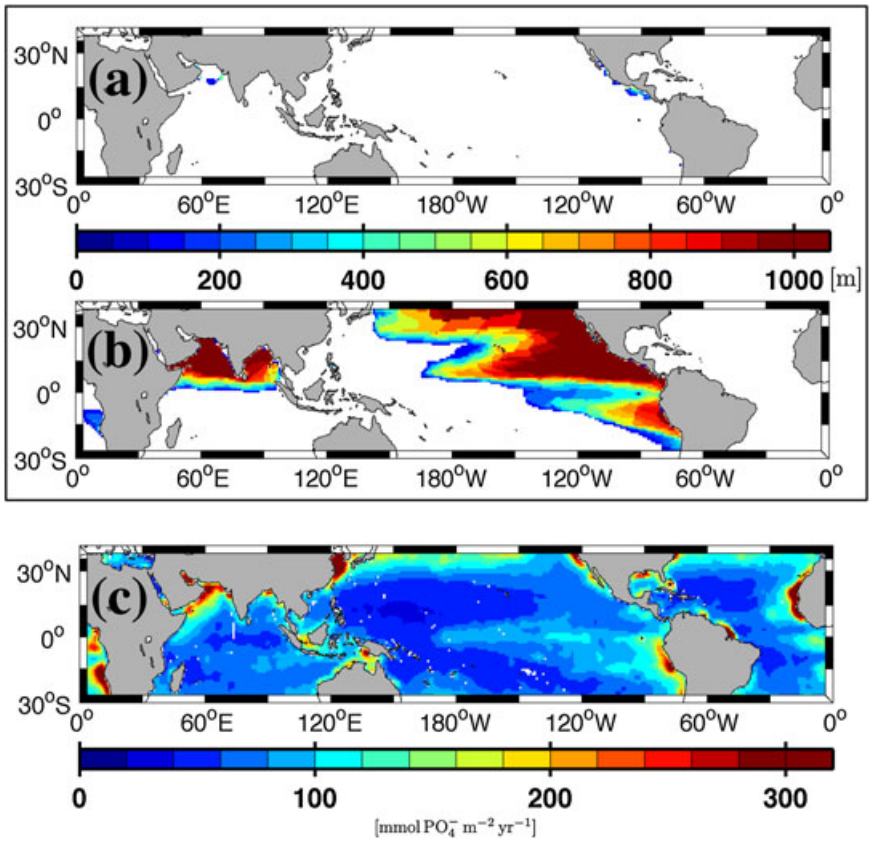

Figure 4. Suboxic fraction of the water column and photosynthetic rates. (a) Depth *interval* which hosts water with oxygen concentrations less than 4.5 mmol O_2 m^{-3} as derived from WOA 2009 observations [*Garcia et al.*, 2010a]. (b) Thought experiment mimicking the effect of a deficient model: same as (a) but based on WOA 2009 oxygen concentrations which are depleted by an additional, imaginary, remineralization corresponding to a 10% increase of observed WOA 2009 PO_4^{3-} concentrations [*Garcia et al.*, 2010b], assuming a Redfield ratio of –160 mol O_2 (mol P)$^{-1}$. (c) Photosynthetic rates derived from satellite-based chlorophyll concentration by *Behrenfeld and Falkowski* [1997].

which was not assessed against observations, might decouple nutrient supply to the euphotic zone from local remineralization of POM at depth, just as an unrealistically high DOM compartment would.

[15] There is a side aspect to the similarity between POM and DOM as regards their capacity to decouple nutrient supply to the surface from local remineralization at depth. That is, in models without an explicit representation of POM, its decoupling role described above has to be taken over, or mimicked by DOM. Hence, we are left uncertain on the question of how much of the supposedly excessive DOM pool must be understood as a proxy for POM in model frameworks similar to the one of *Najjar et al.* [1992] and *Maier-Reimer* [1993].

1.1.2. The Associated Oxygen Problem

[16] *Aumont et al.* [1999] presented a model solution where the bias between simulated phosphate concentrations and observations is below 15%. This is impressive compared to the bias of up to 50% reported by *Najjar et al.* [1992] and *Maier-Reimer* [1993]. However, we argue that even a supposedly small bias of 10% in simulated subsurface phosphate concentrations transfers into a huge error of the area hosting suboxic conditions below the surface (assuming that most of the bias is effected by increased accumulated remineralization, in contrast to be effected by spurious preformed values). This, in turn, effects an increase of that fraction of the global export production that is denitrified. The following gedankenexperiment highlights the scale of the problem.

[17] Assuming that denitrification occurs in suboxic regions defined by a 4.5 mmol O_2 m^{-3} threshold (note that this is similar to what is used in state-of-the-art models) [e.g., *Keller et al.*, 2012], the WOA oxygen climatology [*Garcia et al.*, 2010a] suggests that denitrification in the Pacific is restricted to an area of $\approx 6 \times 10^5$ km^2 close to the American coast, with a vertical *extent* of less than 500 m (the barely visible, colored regions in Figure 4 a). A comparison with photosynthetic rates derived from satellite-based chlorophyll concentration (Figure 4 c) reveals no evidence that suboxia is correlated with unusually high export production and associated rates of oxygen utilization. Hence, in the real ocean, sites of pelagic denitrification are set by a combination of rather low (although significant) export production and a sluggish circulation and unusually low ventilation [e.g., *Karstensen et al.*, 2008].

[18] In contrast, a model which features a realistic ocean circulation and surface nutrient distribution, but which is

biased high by 10% in phosphate at depth, would have an oxygen distribution O_2^{biased}, given by

$$O_2^{biased} = O_2^{WOA} + R_{O_2:P} \times 0.1 \times PO_4^{WOA}, \quad (1)$$

O_2^{biased} is the oxygen climatology O_2^{WOA} reduced by an oxygen consumption corresponding to a 10% increase (hence the factor 0.1 in equation (1)) of remineralized phosphate $\left(PO_4^{WOA}\right)$ at depth. $R_{O_2:P}$ is the O_2 : PO_4^{3-} Redfield ratio ($-160\,mol\,O_2\,(mol\,P)^{-1}$). Figure 4b shows the vertical extent of suboxia diagnosed from O_2^{biased}. A comparison with Figure 4a reveals the relation between a spurious increase of remineralization at depth and spuriously increased areas hosting favorable conditions for pelagic denitrification: the 10% bias in phosphate translates to an increase of suboxic areas by two orders of magnitude. Maybe more important, they now also cover areas with especially high photosynthetic rates and associated export production. This increased export reaching suboxic zones feeds an unrealistically high denitrification. In addition, the spurious suboxia may well retard the sensitivity of denitrification toward circulation changes (as effected by, e.g., a changing climate) since the suboxia hosting the lion's share of the denitrification is set by extraordinary high rates of export production rather than by a sluggish circulation as is the case in the real ocean.

2. Method

[19] In order to explore the "nutrient trapping" problem, we set up a suite of coupled biogeochemical ocean circulation models and define a metric that describes the problem quantitatively.

2.1. Model Simulations

[20] We define our reference simulation "REF" as the global ocean and ice model configuration that has settings that correspond to those used by the Geophysical Fluid Dynamics Laboratory (GFDL) in their coupled climate model CM2.0 [*Gnanadesikan et al.*, 2006]. We do not use a free atmosphere but prescribe conditions at the air-sea boundary following the Coordinated Ocean Reference Experiments (CORE, based on the work of *Large and Yeager* [2004]).

[21] Biogeochemical cycles or ecological interactions are simulated by coupling, online, a nutrient-phytoplankton-zooplankton-detritus (N-P-Z-D) type model similar to the one described in *Oschlies and Garçon* [1999] to the circulation model. Detailed descriptions are given in Appendix A. The model's "base currency" is phosphorous, i.e., the essential limiting macronutrient is phosphate. Dissolved oxygen is coupled via a constant factor to phosphate uptake and remineralization and is exchanged across the air-sea interface.

[22] The reference simulation "REF" is compared with an exhaustive number of combinations of circulation models and biogeochemical models. The focus is on "nutrient trapping." In total, we compare 73 model simulations including five different spacial grids. The suite comprises coarse to high vertical and horizontal resolutions (Table 1), different parameters associated with physical parameterizations, different forcing, and a variety of N-P-Z-D model formulations such as differing parameters (relative to those listed in Table 2), differing formulations of POM sinking, and additional dissolved organic phosphorous compartment (Table 3).

[23] The approach used in this study differs from that of *Najjar et al.* [1992], *Maier-Reimer* [1993], and others in that we do not run our simulations to steady state. After a 20 year spin-up of the circulation model, we integrate, starting from observed climatological fields of phosphate and oxygen [*Garcia et al.*, 2010a, 2010b], the coupled model for another 20 years. Deviations (or misfits) from the initial (and observed) conditions which emerge in the course of the latter integration period are interpreted as indicative of a deficient model formulation. This approach is based on pragmatism since it saves computational cost and makes the interpretation of simulated misfits easier. Easier—because the misfit are associated with deficiently simulated processes acting on relatively short (i.e., order of decades or less) time scales. Hence, any "nutrient trapping" showing up in our simulations cannot, to first order, be caused by deficient convergence of abyssal oxygen and nutrient concentrations associated with the meridional overturning circulation. Neither can "nutrient trapping" be masked by biases of surface oxygen and nutrient concentrations (i.e., by deficient preformed nutrients and oxygen, compare *Duteil et al*. [2012).

2.2. "Nutrient Trapping" Related Metrics

[24] The focus of this study is on "nutrient trapping," i.e., spuriously enhanced subsurface nutrient concentrations in the eastern equatorial Pacific. This region has been addressed by many studies with backgrounds in atmospheric, physical oceanography, and biogeochemical modeling. Each discipline defines its region of interest differently. But as shown in Figure 1, they overlap. In this study, we define the "nutrient trapping region" as that of *Aumont et al.* [1999], while air-sea heat fluxes are averaged over the Ninõ-3 region, and upwelling is integrated over the "upwelling box" of *Wyrtki* [1981]. This is a pragmatic decision, making the comparison with published estimates easier.

[25] The "nutrient trapping" problem has an oxygen counterpart because the remineralization of nutrients is generally accompanied by uptake of oxygen. In the "nutrient trapping region," the relationship between nutrient and oxygen misfits is especially tight and, due to shallow surface mixed layer depths, holds up to the depth of the euphotic zone (Figure 5). Because of its association to the nitrogen cycle (via denitrification), we use the suboxic volume hosted in the "nutrient trapping region" as a measure of "nutrient trapping" in our simulations rather than the nutrient concentrations themselves.

[26] As shown by *Najjar et al.* [1992], the "nutrient trapping" problem is apparently inversely related to the standing stock of DOM at the surface. In section 1.1, we argued that not only DOM but also all standing stocks of all "nutrient carrying" compartments which are subject to advection can reduce the problem because they all decouple local export production from the local supply of nutrients to the euphotic zone. Since in our simulations, phosphate is the essential macronutrient limiting primary production and subsequent export production, we expect that *total* phosphorous at the surface in the "nutrient trapping region" is a relevant parameter associated with "nutrient trapping."

Table 1. Spacial Grids of Models Used in This Study[a]

Name	Number in Table 3	Plot Symbol in Figures 8–11 and 13	Number of Grid Points	Zonal Resolution	Meridional Resolution	Vertical Levels Above 100 m Depth	Forcing	Reference (Similar to)
REF	6	big circle	120 × 65 × 28	3°	3° increasing at 20° latitude to 0.6° at 0°N	9	CORE	*Griffies et al.* [2005]; *Gnanadesikan et al.* [2006]; *Zamora et al.* [2010]
EDDY	42	square	1440 × 369 × 59	0.25°	0.25° increasing to 2° poleward of 30° latitude	10	ERA-40	*Dietze et al.* [2009]; *Liu et al.* [2010]; *Dietze and Kriest* [2012]
DZ20	43	left-pointing triangle	480 × 325 × 35	0.75°	0.75° at the poles, increasing to 0.3° at 0°N	3	CORE	*Griffies et al.* [2005]; *Gnanadesikan et al.* [2006]; *Zamora et al.* [2010]
DZ60	44	right-pointing triangle	480 × 325 × 38	0.75°	0.75° at the poles, increasing to 0.3° at 0°N	2	CORE	*Griffies et al.* [2005]; *Gnanadesikan et al.* [2006]; *Zamora et al.* [2010]
UVic	47	hexagon	100 × 100 × 19	3.6°	1.8°	2	coupled	based on *Weaver et al.* [2001] used in the configuration described by *Schmittner et al.* [2008]

[a]The model numbers refer to numbering in Table 3.

Table 2. Parameters of the Biogeochemical Model as Set in the Reference Simulation[a]

Parameter	Symbol	Value	Units
Phytoplankton (P) Coefficients			
Initial slope of *P-I* curve	α	0.025	$d^{-1}/(W\,m^{-2})$
Maximum growth rate	a	0.6	d^{-1}
e-folding temperature of biotic rates	T_b	15.65	°C
Half-saturation constant for phosphate uptake	k_{PO_4}	0.0312	$mmol\,m^{-3}$
Specific mortality rate of (non nitrogen-fixing) phytoplankton	μ_P	0.03	d^{-1}
Zooplankton (Z) Coefficients			
Assimilation efficiency	γ_1	0.75	
Maximum grazing rate	g	2.0	d^{-1}
Prey capture rate	ϵ	256	$(mmol\,m^{-3})^{-2}\,d^{-1}$
(Quadratic) mortality	μ_Z	51.2	$(mmol\,m^{-3})^{-2}\,d^{-1}$
Excretion	γ_2	0.03	d^{-1}
Detrital (D) Coefficients			
Remineralization rate	μ_D	0.05	d^{-1}
Sinking speed at surface	w_{D_0}	7	m d–1
Increase of sinking speed with depth	m_w	0.04	d^{-1}
Maximum sinking speed in water column	w_{Dmax}	40	m d–1
Dissolved Organic Phosphorous (DOP) Coefficients			
Decay of D to DOP	μ_{D_2}	0	d^{-1}
Decay of DOP to N	μ_{DOP}	0	d^{-1}
Oxygen (O_2) Coefficients			
O_2 to phosphorous ratio	$R_{O_2:P}$	–160	$mol\,O_2\,(mol\,P)^{-1}$

[a]Corresponding to REF in Table 1 and number 6 in Table 3.

[27] In addition to the suboxic volume and total phosphorous at the surface, we use, e.g., sea surface temperature, upwelling, air-sea heat fluxes, the strength of the Equatorial Undercurrent (EUC), and phosphorous transport associated with the EUC, to explore major aspects and underlying mechanisms of the "nutrient trapping" problem.

3. Model Results

[28] We start with a description of "nutrient trapping" in the reference simulation (section 3.1) and continue with a description of our attempts to solve the problem in section 3.2. We distinguish between changes applied to the the N-P-Z-D model (section 3.2.1) and those applied to the circulation model (section 3.2.2)

3.1. "Nutrient Trapping" in the Reference Simulation

[29] Figure 6 shows a zonal section of observed PO_4^{3-} and O_2 concentrations, meridionally averaged between 5°S and 5°N, along with results from the reference simulation: in the deep eastern equatorial Pacific, simulated PO_4^{3-} concentrations are biased high up to 30%. Coupled to this "nutrient trapping" is a massive and likewise spurious overestimation of regions hosting low-oxygenated water. The simulation is not run to equilibrium, and hence, this accumulation of nutrients and associated oxygen depletion is an ongoing process. In the "nutrient trapping region," this corresponds to 3.5 kmol P s^{-1} and –432 kmol O_2 s^{-1}, respectively (reflecting almost, although not exactly, the P : $-O_2$ ratio of 160 prescribed in the N-P-Z-D model). A comparison with in and outbound phosphorous fluxes in Figure 7 puts these numbers into perspective: most of the phosphorous supply to the "nutrient trapping region" comes from the EUC (+25 kmol P s^{-1}) entering the region at 130°W between 75 and 300 m (black line in Figure 7a). This influx is, at these depths, predominantly balanced by upwelling across 75 m (dashed gray line in Figure 7a). Above 75 m, the upwelled nutrients leave the region flowing southward (green line in Figure 7a) and eastward (black line in Figure 7a) with the South Equatorial Current. The residuum, or divergence of all fluxes (red line in Figure 7) includes the effect of the simulated biogeochemistry: biota remove nutrients in the light-lit upper ocean and supply nutrient via sinking particles at depth with the net effect changing sign at apparently 75 m. (Note that this interpretation implicitly assumes steady state, which is a reasonable assumption at the surface but not at depth given the short simulation time.) Deeper down in the water column, between 300 and 2000 m, the budget is dominated by alternating zonal currents crossing 130°W (Figure 7b). The associated transports are substantial amounting to, e.g., a loss of 8 kmol P s^{-1} between 300 and 600 m and a gain of 3 kmol P s^{-1} between 600 and 1100 m.

3.2. Attempts to Fix the "Nutrient Trapping" Problem

[30] Figure 8 summarizes our attempts to fix the "nutrient trapping" problem by comparing respective simulated suboxic volumes at depth and total phosphorous concentrations at the surface with observations.

[31] The observations indicate that there is no suboxic water [e.g., *Garcia et al.*, 2010a] in the "nutrient trapping" region. The total phosphorous concentrations comprise phosphate, dissolved and particulate organic phosphorous. In the following, we try to constrain their concentrations at the surface.

[32] Phosphate is 0.63 ± 0.2 mmol P m^{-3} according to the objectively analyzed annual climatology WOA 2009 [*Garcia et al.*, 2010b]. The associated error refers to

Table 3. List of Simulations

Number	Description
1	Identical to **6**, but phytoplankton growth is reduced down to 10% whenever simulated surface PO_4 drop below observed climatological values of *Conkright et al.* [2002a]. This mimics iron limitation which is not explicitly resolved.
2	Identical to **1**, but reduction occurs when simulated surface PO_4 drop below values corresponding to two times the observed climatological values. This mimics an iron limitation that is more stringent than actual condition.
3	Identical to **1**, but reduction occurs when simulated surface PO_4 drop below values corresponding to three times the observed climatological values. This mimics an iron limitation that is way more stringent than actual conditions.
4	Identical to **1**, but reduction occurs when simulated surface PO_4 drop below values corresponding to four times the observed climatological values. This mimics an iron limitation that is way more stringent than actual conditions.
5	Identical to **1**, but reduction occurs when simulated surface PO_4 drop below values corresponding to five times the observed climatological values. This mimics an iron limitation that is way more stringent than actual conditions.
6	**Reference physics (REF in Table 1), reference biogeochemistry (Table 2)**
7	Identical to **1**, but with an additional dissolved organic phosphorous (DOP) compartment and associated parameters (equation (A6)) $\mu_{D_2} = 0.05\,d^{-1}$ and $\mu_{DOP} = 0.0037\,d^{-1}$.
8	Identical to **6**, but lower (compare Table 2) maximum phytoplankton growth rate $a = 0.05\,d^{-1}$.
9	Identical to **6**, but $a = 0.3\,d^{-1}$.
10	Identical to **6**, but $a = 0.27\,d^{-1}$.
11	Identical to **6**, but $a = 0.29\,d^{-1}$.
12	Identical to **6**, but $a = 0.31\,d^{-1}$.
13	Identical to **6**, but $a = 0.33\,d^{-1}$.
14	Identical to **6**, but $a = 0.2\,d^{-1}$.
15	Identical to **6**, but $a = 0.12\,d^{-1}$.
16	Identical to **6**, but faster (compare Table 2) remineralization of detritus, $\mu_D = 0.1\,d^{-1}$.
17	Identical to **1**, but $\mu_D = 0.1\,d^{-1}$.
18	Identical to **6**, but with an additional dissolved organic phosphorous (DOP) compartment and associated parameters (equation (A6)) $\mu_{D_2} = 0.05\,d^{-1}$ and $\mu_{DOP} = 0.00667\,d^{-1}$.
19	Identical to **6**, but $\mu_{D_2} = 0.05\,d^{-1}$, $\mu_{DOP} = 0.0037\,d^{-1}$.
20	Identical to **19**, but with photosynthetically active radiation (PAR) artificially reduced down to 50%.
21	Identical to **19**, but with PAR increased artificially up to 200%.
22	Identical to **6**, but with an additional dissolved organic phosphorous (DOP) compartment and associated parameters (equation (A6)) $\mu_{D_2} = 0.05\,d^{-1}$ and $\mu_{DOP} = 0.033\,d^{-1}$.
23	Identical to **6**, but $\mu_{D_2} = 0.04\,d^{-1}$ and $\mu_{DOP} = 0.00667\,d^{-1}$.
24	Identical to **6**, but $\mu_{D_2} = 0.033\,d^{-1}$ and $\mu_{DOP} = 0.00667\,d^{-1}$.
25	Identical to **6**, but $\mu_{D_2} = 0.0166\,d^{-1}$ and $\mu_{DOP} = 0.00667\,d^{-1}$.
26	Identical to **6**, but $\mu_{D_2} = 0.0166\,d^{-1}$ and $\mu_{DOP} = 0.0037\,d^{-1}$.
27	Identical to **6**, but $\mu_{D_2} = 0.0166\,d^{-1}$ and $\mu_{DOP} = 0.033\,d^{-1}$.
28	Identical to **6**, but faster (compare Table 2) remineralization of detritus $\mu_D = 0.2\,d^{-1}$ which is even faster than in **16**.
29	Identical to **1**, but faster (compare Table 2) remineralization of detritus $\mu_D = 0.2\,d^{-1}$.
30	Identical to **6**, but lower quadratic mortality of zooplankton $\mu_Z = 25.6(\text{mmol}\,m^{-3})^{-2}\,d^{-1}$.
31	Identical to **6**, but with $\mu_Z = 0.08\,d^{-1}$.
32	Identical to **6**, but with $\mu_Z = 0.4\,d^{-1}$.
33	Identical to **6**, but with $\mu_Z = 0.133\,d^{-1}$.
34	Identical to **6**, but with detritus not sinking at all at the surface ($w_{D_0} = 0\,m\,d^{-1}$) and a slower increase of the sinking velocity with depth $m_w = 0.01\,d^{-1}$.
35	Identical to **6**, but with $w_{D_0} = 0\,m\,d^{-1}$ and $m_w = 0.02\,d^{-1}$.
36	Identical to **6** but with $w_{D_0} = 0\,m\,d^{-1}$ and $m_w = 0.04\,d^{-1}$.
37	Identical to **6** but with $w_{D_0} = 5\,m\,d^{-1}$ and $m_w = 0.02\,d^{-1}$.
38	Identical to **6**, but critical Richardson number in KPP scheme [*Large et al.*, 1994] changed from 0.3 to 0.05 which should result in shallower surface mixed layer depths.
39	Identical to **6**, but critical Richardson number in KPP scheme is 0.1.
40	Identical to **6**, but critical Richardson number in KPP scheme is 0.4 which should result in deeper surface mixed layer depths.
41	Identical to **6**, but critical Richardson number in KPP is 1.
42	The biogeochemical model is identical to the one in **1**, but the circulation model (**EDDY** in Table 1) features an eddy-permitting horizontal resolution, a higher vertical resolution, and ERA-40 forcing (section 1.1.2).
43	The biogeochemical model is identical to the one in **1**, but the circulation model (**DZ20** in Table 1) features differing horizontal and vertical resolutions.
44	Identical to **43**, but with a coarser vertical resolution dubbed **DZ60** in Table 1.
45	DZ20 (Table 1) circulation model combined with a biogeochemistry identical to that in **19** (i.e., with an explicit representation of DOP).
46	DZ60 (Table 1) circulation model combined with a biogeochemistry identical to that in **19** (i.e., with an explicit representation of DOP).
47	**UVic** model as described in *Schmittner et al.* [2008] (Table 1).
49	Identical to **6**, but with detritus sinking speed $w_{D_0} = 1\,m\,d^{-1}$ being very low (compare Table 2) and constant with depth $m_w = 0\,d^{-1}$.
50	Identical to **6**, but with detritus sinking speed $w_{D_0} = 10\,m\,d^{-1}$ being rather high (compare Table 2 and constant with depth $m_w = 0\,d^{-1}$).
51	Identical to **6**, but with $w_{D_0} = 2\,m\,d^{-1}$ and $m_w = 0\,d^{-1}$.
52	Identical to **6**, but with $w_{D_0} = 40\,m\,d^{-1}$, $m_w = 0\,d^{-1}$.
53	Identical to **6** but with wind stress (that drives the ocean circulation) reduced globally down to 75%.

(continued on next page)

Table 3. (continued).

Number	Description
54	Identical to **6**, but with wind stress increased globally up to 125%.
55	Identical to **6**, but with wind stress increased globally up to 150%.
56	Identical to **6**, but biogeochemical tracers are advected with upstream numerics [compare *Oschlies*, 2000]. Temperature, salinity, and momentum are advected the Sweby numerics [*Hundsdorfer and Trompert*, 1994; *Sweby*, 1984], as is the case for all prognostic tracers in **6**.
57	Identical to **1**, but with wind stress reduced globally down to 75%.
58	Identical to **1**, but with wind stress increased globally up to 125%.
59	Identical to **1**, but with wind stress increased globally up to 150%.
60	Identical to **1**, but nutrients are artificially restored to zero within the EUC between 135°W and 130°W with a time scale of 1 month which reduces the EUC phosphate load down to 50%.
61	Identical to **1**, but nutrients are artificially restored to zero within the EUC between 135°W and 130°W with a time scale of 1 year.
62	Identical to **1**, but climatological chlorophyll values which are used to calculate the absorption of solar shortwave radiation heating the ocean are increased by a factor of 10.
63	Identical to **1**, but climatological chlorophyll values which are used to calculate the absorption of solar short wave radiation heating the ocean are set to 0.
64	Identical to **6**, but isopycnal diffusivity (which parameterizes the effect of unresolved circulation) is reduced from an initial 1000 down to 500 $m^2 s^{-1}$.
65	Identical to **6**, but isopycnal diffusivity is doubled to 2000 $m^2 s^{-1}$.
66	Identical to **6**, but isopycnal diffusivity is increased by a factor of 5 up to set to 5000 $m^2 s^{-1}$.
67	Identical to **6**, but a vertical background diffusivity of 5 $cm^2 s^{-1}$ is added throughout the water column.
68	Identical to **6**, but the vertical background diffusivity below the surface mixed layer depth is set to 5 $cm^2 s^{-1}$.
69	Identical to **6**, but the vertical background diffusivity below the surface mixed layer depth is set to 1 $cm^2 s^{-1}$.
70	Identical to **6**, but vertical background viscosity is set to 5 $cm^2 s^{-1}$.
71	Identical to **6** but vertical background viscosity is set to 0.5 $cm^2 s^{-1}$.
72	Identical to **6**, but oxygen consumption is increased during remineralization of organic matter, $R_{O_2:P} = -240$ mol O_2 (mol P)$^{-1}$.
73	Identical to **6**, but oxygen consumption is decreased, $R_{O_2:P} = -80$ mol O_2 (mol P)$^{-1}$.

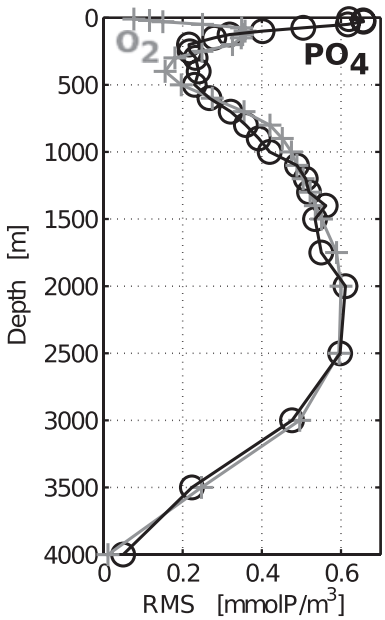

Figure 5. Root mean square (RMS) deviation of the "reference" model simulation (simulation 6 and REF defined in Tables 3 and 1, respectively) from observations [*Garcia et al.*, 2010a, 2010b] calculated for PO_4^{3-} (black lines and circles) and O_2 (gray lines and crosses) within the "nutrient trapping" region. The O_2 RMS deviation is divided by the $R_{O_2:P} = -160$ mol O_2(mol P) Redfield ratio prescribed in the model (Table 2).

typical errors of the statistical mean in the 1° × 1° horizontal bins. The actual uncertainty might be greater than that, given that most bins used to calculate the average over the "nutrient trapping region" host less than two observations. DOP measurements are few and read between 0.05 and 0.3 mmol P m^{-3} according to the Global Open Ocean DOP database (Figure 3). We could not find any particulate organic phosphorous (POP) measurements in the region. The closest we found was a transect from 47.9°N, 166.4°W to 30.8°N, 169.5°E by *Yoshimura et al.* [2007] where POP-scaled linear with Chl*a* in a range from 0.08 to 1.35 mg Chl*a* m^{-3}. Applying their relationship to a chlorophyll concentration of 0.5 mg Chl*a* m^{-3} which is rarely exceeded in the region yields a POP concentration of 0.05 mmol P m^{-3}. Note that these estimates for DOP and POP are consistent with *Abell et al.* [2000] who observed total organic phosphorous surface concentrations short of 0.3 mmol P m^{-3} at 10°N, 158°W.

[33] We conclude, using respective upper and lower bounds of the latter estimates that data, available to date, imply a total surface phosphorous concentration between 0.5 and 1.2 mmol P m^{-3}. This, in turn, implies that all of our simulations feature either "nutrient trapping" or unrealistic high total surface phosphorous concentrations, or both deficiencies. In the following (sections 3.2.1 and 3.2.2), we structure the information shown in Figure 8.

3.2.1. Biogeochemical Sensitivities

[34] Here we use the reference simulation and apply changes to the biogeochemistry only.

[35] Our reference simulation features a spurious accumulation (depletion) of nutrients (oxygen) in the thermocline. Potential solutions to this "nutrient trapping" problem are (1) a reduction of the local export production through, e.g., iron limitation of phytoplankton growth, enhanced top-down control by zooplankton grazing, or a reduction of phytoplankton growth rates. (2) An adjustment of the depth of remineralization of organic matter export (to depth, out of the euphotic zone) by, e.g., changing the sinking speed

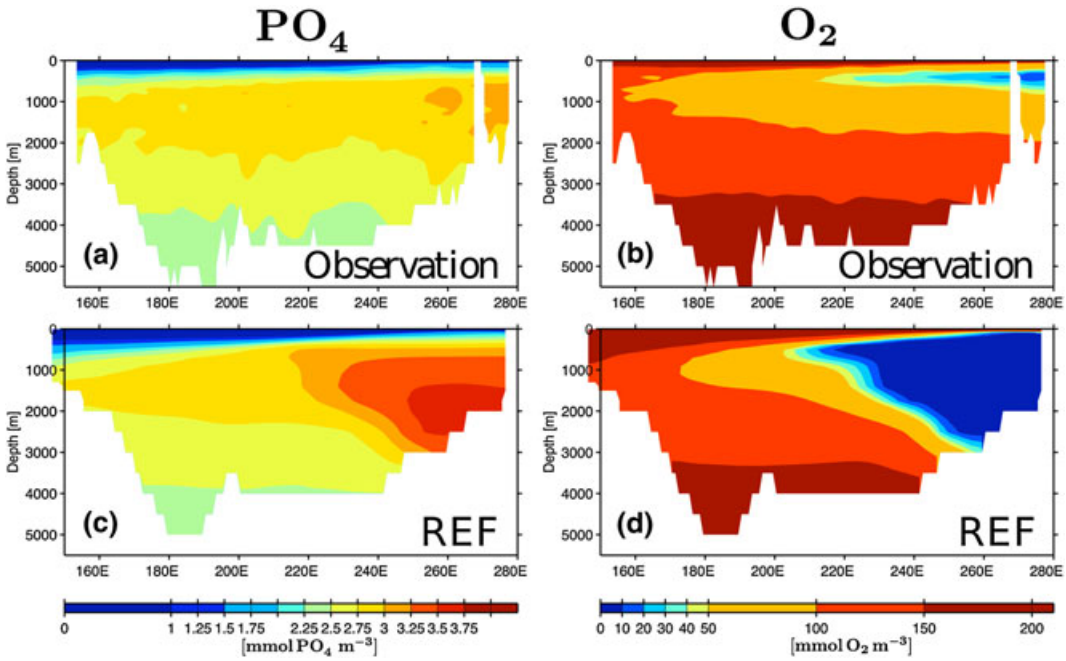

Figure 6. "Nutrient trapping" and its oxygen counterpart. (a and b) Observed (WOA 2009) [*Garcia et al.*, 2010a, 2010b], meridionally averaged (5°S to 5°N) PO_4^{3-} and O_2 concentrations. (c and d) PO_4^{3-} and O_2 as simulated by the reference model (and meridionally averaged).

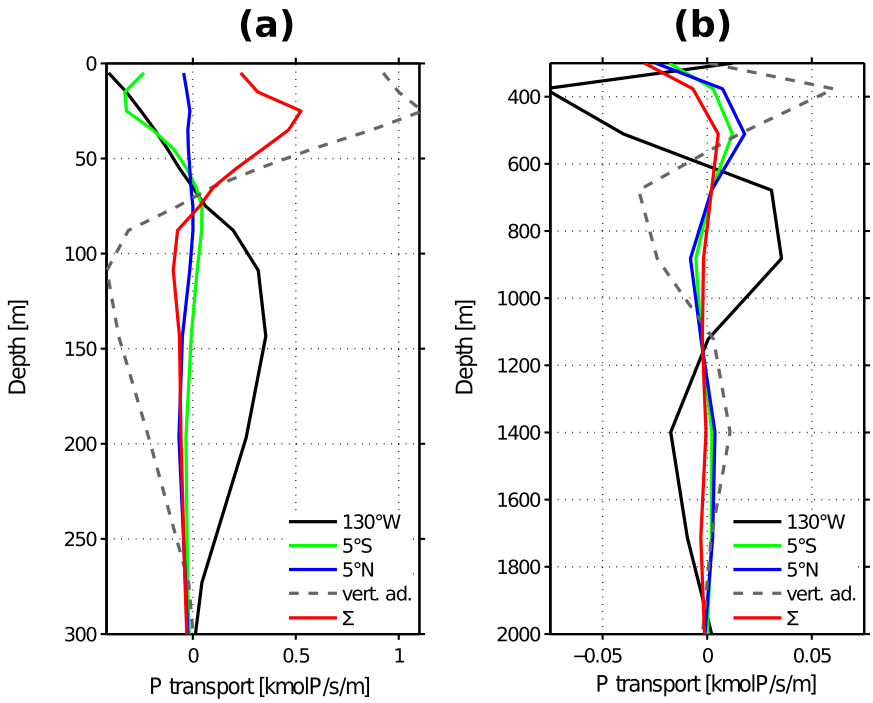

Figure 7. Simulated (reference model, number 6 in Table 3), advective transport budget of total phosphorous for the "nutrient trapping" region. Positive (negative) fluxes correspond to a nutrient gain (loss) within the region at respective depth. The black line refers to zonal fluxes across 130°W integrated meridionally from 5°S to 5°N. The green (blue) line refers to meridional fluxes across 5°S (5°N) integrated zonally from 130°W to the American coast. The dashed gray line denotes the vertical divergence of vertical fluxes integrated over the region. The red line shows the residuum of all advective fluxes. This residuum balances the export of POM at the surface and its remineralization at depth (implicitly assuming steady state and that diffusive fluxes are negligible). (a) and (b) show the upper 300 and 300–2000 m, respectively.

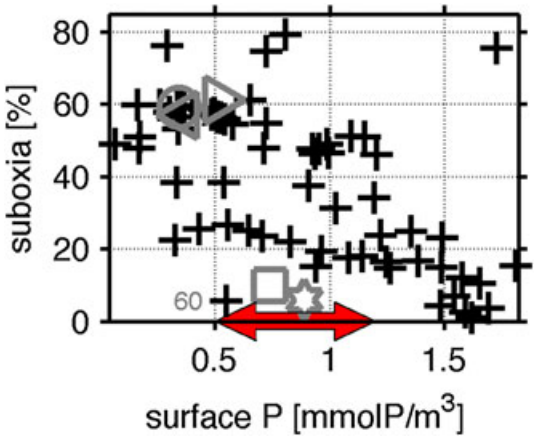

Figure 8. "Nutrient trapping" versus total (including all organic and inorganic forms) phosphorous concentration at the surface in the "nutrient trapping region." "Nutrient trapping," expressed as suboxia, is measured as that fraction of the total volume hosting oxygen concentrations below 4.5 mmol O_2 m^{-3}. The red double arrow marks the observations with zero suboxic volume and an uncertainty associated with the surface total phosphorous as indicated by the arrowheads. Each black + refers to one model simulation. A gray 60 labels simulation number 60 as defined in Table 3, and the reference simulation is denoted by a gray circle. Other gray symbols are defined in Table 1.

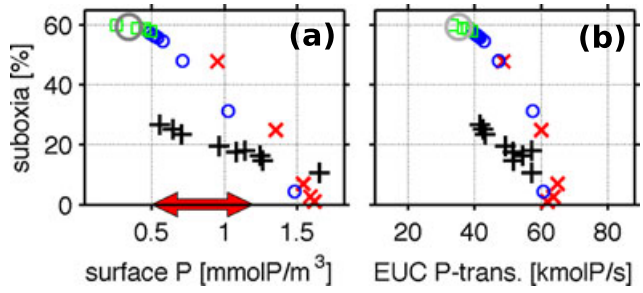

Figure 9. "Nutrient trapping"—effects of DOP, iron, growth, and grazing. (a) A subset of data shown in Figure 8. The gray circle denotes the reference simulation (number 6 in Table 3), black pluses refer to altered DOP dynamics (numbers 7, 18, 19, 22–27 in Table 3), red crosses denote simulations where various levels of iron limitation are mimicked (numbers 1–5 in Table 3), blue circles refer to various phytoplankton growth rates (number 8–15 in Table 3) and the green squares refer to simulations with differing zooplankton grazing pressure (numbers 30–33 in Table 3). The red double arrow marks the observations with zero suboxic volume and an uncertainty associated with the surface total phosphorous as indicated by the arrowheads. (b) The percentage of suboxic volume as a function of phosphorous supply (to the "nutrient trapping" region) associated with the Equatorial Undercurrent.

of particulate organic matter (POM) or its remineralization time scale, or by introducing dissolved organic matter (DOM) which does not sink at all. In addition, any of these adjustments or combinations thereof might alter the nutrient (oxygen) concentrations outside the "nutrient trapping region." This, in turn, may change the allochthonous nutrient supply to the region and ultimately the export production and associated remineralization at depth.

[36] Figures 9a and 10a evaluate the potential solutions discussed above: in all cases, decreased "nutrient trapping" is correlated with increased total phosphorous (P) concentrations at the surface. Further, the "nutrient trapping" vanishes (i.e., suboxia approaching zero) only if surface P is well beyond the range of observational estimates. This means that changes applied to the biogeochemical model can (by increasing the surface phosphorous concentration of water flushed out of the region) reduce "nutrient trapping," but only to a certain degree.

[37] Figures 9b and 10b explain why the effect of increasing total surface phosphorous on suboxia cannot resolve the problem completely. The figures show simulated suboxia as a function of phosphorous supplied to the "nutrient trapping region" by the EUC. Apparently they are inversely correlated with one another. Hence, we conclude from Figures 9 and 10 that fairly independent of the details of changes applied to the biogeochemical model, increased surface P comes along with both reduced suboxia and increased P supply associated with the EUC. This increased P supply, however, favors "nutrient trapping" because part of it is branched to the euphotic zone where it can fuel export production.

[38] In summary, we find that (1) surface P, increased by decreasing the export efficiency of the biogeochemical model, is (according to Figure 7) flushed by approximately equal parts to the south and west, out of the region. This shifts export production away from the "nutrient trapping region" and reduces "nutrient trapping." (2) That fraction leaving the region to the west via the South Equatorial Current will, sooner or later, on its way westward across the basin, fuel export production. Part of this export will be remineralized in the EUC thereby increasing its nutrient load. (3) The EUC entering the "nutrient trapping region" will drive an increased nutrient supply. (4) Because the EUC feeds the upwelling, its increased nutrient concentration will increase the nutrient supply to the surface. (5) This, in turn, can drive additional local export production causing additional "nutrient trapping."

[39] Changing the biogeochemical model coupled to other ocean circulations models (e.g., runs 43, 45 and 44, 46 in Table 3) yielded similar results. These results are included in Figure 8 but not explicitly discussed for the sake of brevity.

3.2.2. Circulation Sensitivities

[40] Here, we present the effects of modified ocean circulation models on "nutrient trapping." To this end, we increase (as suggested by *Aumont et al.* [1999]) the horizontal resolution up to 0.25°, test a range of vertical resolutions as suggested by *Maier-Reimer* [1993] (compare Table 1), and explore uncertainties related to the wind stress which drives the massive upwelling in the region. In addition, horizontal isopycnal diffusivities, viscosities, and parameters associated with the surface boundary layer parameterization are modified. All these changes are applied to the reference biogeochemical model except in two cases: (1) In the configuration "UVic," the biogeochemistry is as described in *Schmittner et al.* [2008]. (2) In the configuration "EDDY"

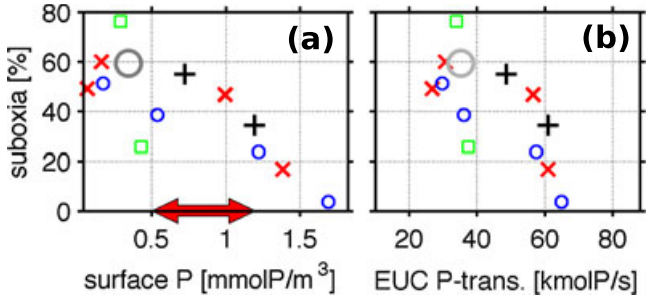

Figure 10. "Nutrient trapping"—effects of sinking and remineralization of detritus. (a) A subset of data shown in Figure 8. The gray circle denotes the reference simulation (number 6 in Table 3), black pluses refer to altered remineralization time scales (numbers 16 and 28 in Table 3), the red crosses to differing sinking speeds set constant with depth (numbers 49–52 in Table 3), and the blue circles to modified vertical profiles of sinking speed (numbers 34–37 in Table 3). The green squares refer to modified stoichiometries (numbers 72 and 73 in Table 3). The red double arrow marks the observations with zero suboxic volume and an uncertainty associated with the surface total phosphorous as indicated by the arrowheads. (b) The percentage of suboxic volume as a function of phosphorous supply (to the "nutrient trapping" region) associated with the Equatorial Undercurrent.

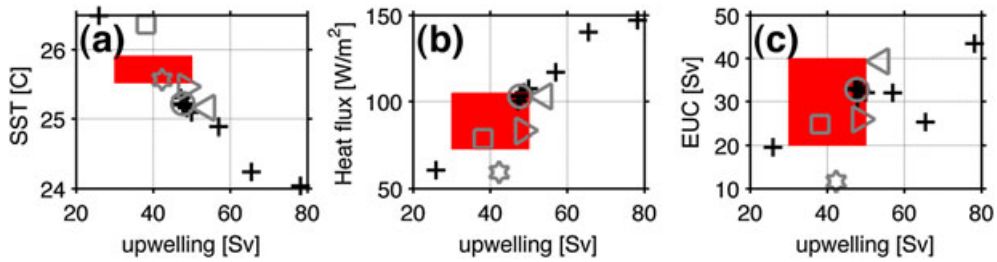

Figure 11. (a) Sea surface temperature, (b) air-sea heat flux, and (c) EUC volume transport as a function of upwelling. All properties are averaged or integrated over regions defined in Figure 1. The red patches indicate respective ranges of observational estimates (Appendix C). The black pluses refer to simulations 53, 54, and 64–71 defined in Table 3. Gray symbols refer to simulations run on differing spacial grids defined in Table 1.

(Table 1), the phytoplankton growth rate is reduced whenever simulated surface phosphate concentration falls short of observed climatological monthly concentrations [*Garcia et al.*, 2010b]. This mimics iron limitation which is not explicitly included. In all other aspects, the biogeochemical model configuration is identical to that used in the reference simulation.

[41] Modifications to the circulation alter the upwelling of relatively cold water to the surface. This affects sea surface temperature and air-sea heat fluxes. Figures 11a and 11b show that these relationships are almost linear in our simulations: an increased upwelling results in reduced sea surface temperatures and an increased air-sea heat flux entering the ocean. Figure 11c shows another, although weaker, relationship between the upwelling and the EUC transport, where increased upwelling is correlated with an increased EUC volume transport. This correlation is consistent with an EUC that shoals on its way east across the Pacific. Indeed, both observations and all simulations (except for UVic) feature this eastward shoaling as shown in Figure 12.

[42] As regards the weakest "nutrient trapping" combined with realistic surface phosphorous concentrations, three simulations rank equal according to Figure 8. These are EDDY, UVic (Table 1), and simulation number 60 (Table 3). All of them are, however, inconsistent with one or more sets of observations as shown in Figure 11:

[43] 1. Simulation number 60 is a special and artificial case because it was designed to understand the connection between suboxia and phosphorous transport associated with the EUC. To this end, the EUC's phosphate concentration was artificially halved by a restoring condition. This, by no means, parameterizes a realistic process and reduces phosphate concentrations in the EUC below realistic values.

[44] 2. The simulation UVic features realistic sea surface temperatures and upwelling. Its air-sea heat flux seems too low but then we were unsure how to compute the observational error of the fluxes (Appendix C). The simulation UVic is, however, inconsistent with estimates of the EUC volume transport which it massively underestimates. Because of the dominant role of the EUC in the region, this raises doubt if the models' good representation of other metrics is caused by realistic dynamics.

[45] 3. The simulation EDDY features realistic upwelling, EUC transport, and air-sea heat flux. To this end, it is apparently the most realistic simulation although it features a sea surface temperature which is biased high (Figure 11).

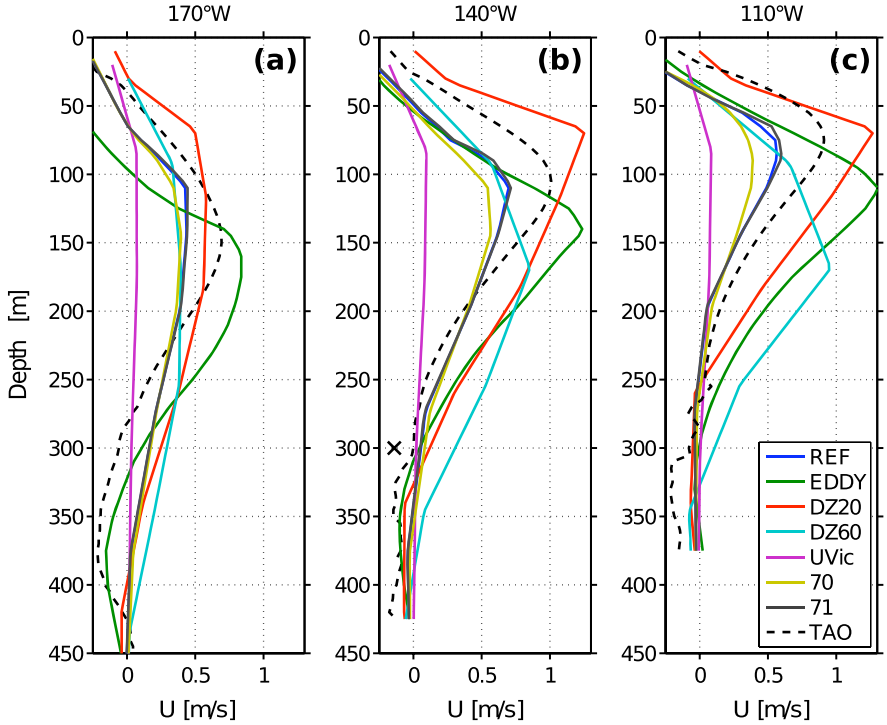

Figure 12. Vertical profiles of zonal velocities at the equator at (a) 170°W, (b) 140°W, and (c) 110°W. Colored lines refer to the simulations defined in Tables 1 and 3. The dashed black lines refer to an average of all ADCP observations contained in the TAO (http://www.pmel.noaa.gov/tao/) data set. The black plus in Figure 12b (referring to 140°W) denotes measurements by mechanical current meters from the same database.

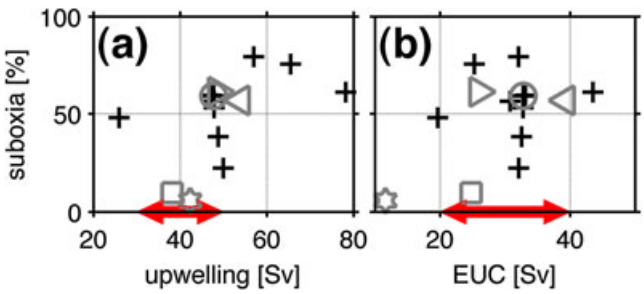

Figure 13. "Nutrient trapping"—effects of the ocean circulation. (a) A subset of data shown in Figure 8. (b) The percentage of suboxic volume as a function of the EUC volume transport. The red double arrows mark the observations with zero suboxic volume and volume transport uncertainties as discussed in Appendix C. The black pluses refer to simulations 53, 54, and 64–71 (defined in Table 3). Gray symbols refer to simulations run on differing spacial grids defined in Table 1.

[46] To summarize, we conclude that the simulations presented in this study cover the range of uncertainties associated with physical processes so far considered to be related to "nutrient trapping" (Figure 11). Nevertheless, all simulations feature "nutrient trapping" (Figure 13). This does even apply to those simulations which overestimate the EUC volume transport, which contradicts a previous study: *Aumont et al.* [1999] argue that a stronger EUC will have a diluting effect on upwelled nutrient concentrations which, in turn, should prevent "nutrient trapping." In contrast, we find a compensating mechanism where a stronger EUC volume transport is associated with stronger upwelling in the "nutrient trapping" region. This enhanced upwelling overrules the diluting effect, brings up more nutrients to the euphotic zone, and fuels enhanced export production and associated "nutrient trapping." Hence, the "nutrient trapping" problem cannot be simply ascribed to a deficient simulation of the EUC volume transport. Somewhat in line with *Aumont et al.* [1999], we find that our high-horizontal-resolution simulation (EDDY) is the most realistic one.

4. Discussion

[47] In the literature, two processes have been proposed to resolve the "nutrient trapping" problem: a deficient representation of the dynamics of dissolved organic matter and an EUC being too weak. While our simulations confirm that these are major processes related to the problem, the new finding here is that their roles are ambiguous. On the one hand, enhanced dissolved organic matter concentrations do shift export production and subsequent nutrient accumulation out of the region. On the other hand, a significant part of the nutrients, associated with DOM flushed out of the region by the SEC, reenters via the EUC at depth. These reentering nutrients are partly upwelled into the euphotic zone and can drive enhanced export production.

[48] Concerning the EUC, it was argued before that a fast EUC will accumulate less remineralized nutrients on its way across the Pacific into the "nutrient trapping" region. This decreases the nutrient concentration of upwelled water, i.e.,

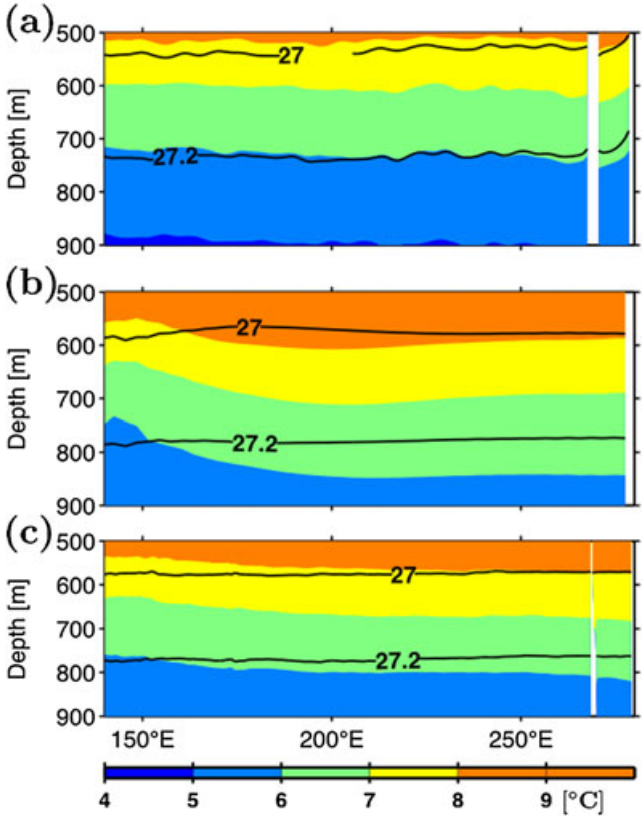

Figure 14. Potential temperature (in color and units °C) and density σ_0 (labeled contours) along the equator. (a) Observations [*Locarnini et al.*, 2010; *Antonov et al.*, 2010] and simulation of (b) REF and (c) EDDY as defined in Table 1.

the nutrient supply to the euphotic zone, and potentially also the local export production. This effect, however, is overruled in our simulations by an increase in upwelling which comes along with increased EUC transport.

[49] Given that the problem is just a tiny residuum (3.5 kmol P s^{-1}, section 3.1) of a budget dominated by huge fluxes (e.g., the inbound 25 kmol P s^{-1} associated with the EUC) in combination with high uncertainties of even physical properties, such as volume transport and heat fluxes, it seems hopeless to pin down the one model deficiency responsible for the "nutrient trapping." Aggravating in that respect is the high complexity of the system where processes tend to have ambiguous effects as outlined above.

[50] Our simulations explore a wide range of circulations and parameterizations of biogeochemical processes. As regards metrics deemed previously important with respect to "nutrient trapping" (e.g., the EUC volume transport), we explore the full range of observational uncertainty and beyond. Even so, "nutrient trapping" persists in all of our simulations. At the same time, tedious comparisons between all simulations reveal the one model deficiency, eye-catching and common to all simulations: strong zonal temperature gradients on isopycnal surfaces, deep down in the water column. Figure 14b shows these gradients as simulated by the reference simulation, which is representative for all simulations. The most realistic simulation, as regards zonal isopycnal gradients, is the eddy-permitting (EDDY) simulation (Figure 14c).

[51] Associated with these spurious zonal isopycnal gradients of temperature is a deficient zonal distribution of phosphate at depth. Figure 15a shows that in all simulations, the spurious accumulation of phosphate in the eastern equatorial Pacific (the so-called "nutrient trapping") comes along with a phosphate deficit of similar magnitude in the western equatorial Pacific. Expressed as a zonal gradient of phosphate relative to the observed gradient, this misfit ranges between 30% (simulation EDDY) and more than 200% (Figure 15b).

[52] The combination of spurious zonal distribution of physical and biogeochemical properties (temperature gradients on isopycnals and phosphate) suggests that a zonal mixing process at depth, below the EUC, is missing in the circulation models. In fact, the equatorial Pacific features the strongest deep zonal currents worldwide, with mean speeds of 0.1–0.15 m s^{-1} (as derived, e.g., from floats) [*Ascani et al.*, 2010; *Cravatte et al.*, 2012]. These currents, dubbed the Equatorial Intermediate Current System (EICS) and Equatorial Deep Jets (EDJs), alternate east- and westward with depth and it is plausible to assume that they mix massively in zonal direction. To date, however, all attempts to model the EICS and EDJs failed or accomplished only a damped representation of the current system. This does even apply to models with a horizontal resolution as high as 0.1° in both zonal and meridional direction [*Ascani et al.*, 2010]. We speculate that at least some of the "nutrient trapping" endemic to today's coupled biogeochemical is caused by a deficient representation of the EICS and EDJs in ocean circulation models. Figure 16 supports this conclusion insofar that the simulation EDDY, which features only relatively modest "nutrient trapping," shows more skill in simulating zonal velocities at depth than the reference simulation which features way more "nutrient trapping."

[53] Note, that the effect of the EICS and EDJs on the zonal distribution of biogeochemical species along the equator has, to our knowledge, not been explicitly stated so far. To this end, it is noteworthy that *Rafter et al.* [2012] conclude, surprised by the zonal uniformity of $\delta^{15}N$ of NO_3^- at depth, that within the equatorial zone, rapid transport processes must be at work.

5. Summary

[54] "Nutrient trapping" can be prevented if local export of organic material to depth is sufficiently decoupled from the local upwelling of nutrients to the sunlit surface of the eastern equatorial Pacific. Early studies [e.g., *Najjar et al.*, 1992] argued that this decoupling can only be achieved by introducing an unrealistically high standing stock of DOM. We argue that this decoupling can also be achieved by introducing unrealistically high (and explicitly simulated) stocks of POM (e.g., phytoplankton, zooplankton, or detritus) which, if not assessed against observations, can conceal the thereby shifted problem. Hence, analyses of "nutrient trapping" should include an assessment of total nutrient, defined as the sum of all nutrient-carrying model compartments which are subject to oceanic circulation and mixing.

[55] From the wide range of circulation models and differing biogeochemical model configurations explored in this

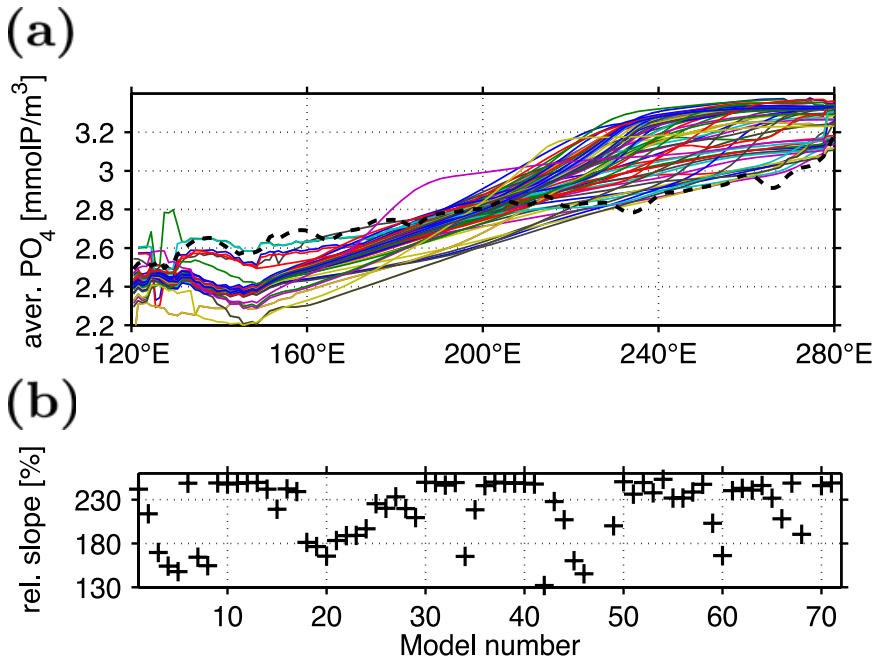

Figure 15. Zonal distribution of PO_4^- in the deep equatorial Pacific. (a) Concentrations averaged over 350–1500 m depth and 5°S to 5°N latitude. The colored lines refer to all model simulations investigated in this study (except for 72 and 73 which, as regards PO_4^-, are almost identical to the reference), the black dashed line denotes observations [*Garcia et al.*, 2010b]. (b) Simulated zonal slopes of the (meridionally and vertically) averaged concentrations relative to the observed slope. The "model numbers" are defined in Table 3. Note that numbers 72 and 73 are not included because they differ only with respect to their phosphorous to oxygen stoichiometry from the reference simulation.

study, a more comprehensive picture of "nutrient trapping" as a persistent problem emerged (schematic in Figure 17). We argue that processes recently thought to ease or resolve the problem such as DOM dynamics or enhanced EUC transport are ambiguous, meaning they are tied to feedback mechanisms opposing their capacity to resolve the problem.

[56] More specifically, we find that a substantial fraction of increased simulated surface DOM concentrations in the "nutrient trapping region" are flushed out of the region via the South Equatorial Current and, ultimately, drive increased POM remineralization in the EUC. Increased nutrient concentrations in the EUC then enhance the nutrient supply to the region which weakens the potential of DOM dynamics to resolve "nutrient trapping." As regards the role of the EUC's strength we find, in contrast to *Aumont et al.* [1999], that the simulation of a stronger EUC does not necessarily resolve "nutrient trapping." A stronger EUC can, due to volume conservation, be related to stronger upwelling which drives additional nutrient fluxes to the sunlit surface. This, in turn, aggravates the problem rather than resolving it.

[57] Finally we speculate that "nutrient trapping" is caused by a deficient representation of the Equatorial Intermediate Current System and Equatorial Deep Jets, at depth, below the EUC, which is a problem endemic even to eddy-resolving circulation models [*Ascani et al.*, 2010]. This speculation is consistent (1) with simulated spurious zonal gradients of phosphate at the equator, (2) with simulated spurious zonal temperature gradients on isopycnal surfaces at the equator, and (3) with simulated zonal velocities being too weak compared to observations at depth.

Appendix A: Model Descriptions

[58] Table 3 lists all simulations.

A1. Ocean Circulation Models

[59] Diffusive and advective fluxes of inorganic nutrients and organic matter are calculated by finite differences, primitive equation ocean general circulation models. Among the simulations are five different spacial grids, all of them covering the entire global ocean (Table 1). Prominent simulations featuring the respective grids are dubbed REF, EDDY, DZ20, DZ60, and UVic.

[60] Further, the simulations comprise three different configurations of atmospheric forcing: (1) The UVic configuration, identical to the one described by *Schmittner et al.* [2008], features prescribed winds and a coupled atmospheric energy-moisture balance model. (2) The configurations REF, DZ20, and DZ60 are driven by the CORE data set [*Large and Yeager*, 2004]. (3) The configuration EDDY is driven by ERA-40 reanalyses from the European Centre for Medium-Range Weather Forecasts [*Uppala et al.*, 2005, and many more to follow].

[61] The configurations REF, DZ20, DZ60, and EDDY are based on the MOM4p0d (GFDL Modular Ocean Model v.4) [*Griffies et al.*, 2005] z coordinate, free-surface ocean general circulation model. UVic is based on MOM2.2.

A1.1. CORE

[62] "CORE" in Table 1 refers to the Corrected Normal Year Forcing fields, version 1.0 (which is based on the work of *Large and Yeager* [2004]). These fields include annual

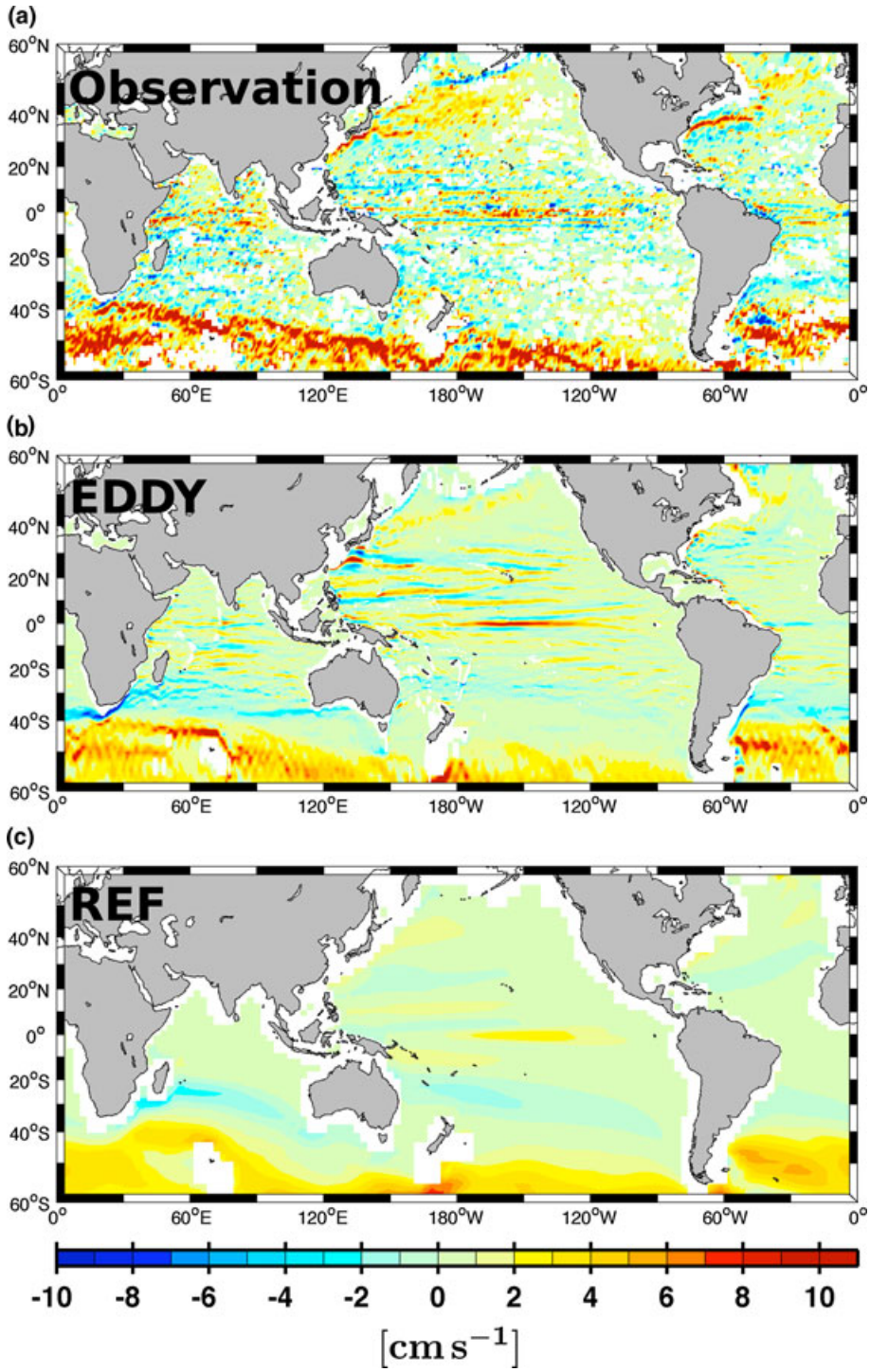

Figure 16. Zonal velocities at 1000 m depth. (a) Velocity data assessed from trajectories of Argo floats at parking level, based on data from *Lebedev et al*., [2007], and reproducing *Ascani et al*., [2010] (their Figure 2). Note that *Cravatte et al.* [2012] published a more detailed view (their Figure 2). Annual means simulated with (b) EDDY and (c) REF as defined in Table 1.

mean river runoff, monthly varying precipitation, daily varying shortwave and longwave radiation, six-hourly varying 10 m atmospheric temperature, humidity, zonal velocity, meridional velocity, and sea level pressure.

[63] All of our simulations that share the "CORE" forcing (Table 1) have settings that correspond to those used by GFDL in their coupled climate model CM2.1 used for the AR4 IPCC report [*Griffies et al.*, 2005; *Gnanadesikan et al.*, 2006]. Results from a similar configuration are published by *Zamora et al.* [2010]. The configurations DZ20 and DZ60 were set up from scratch.

[64] We do not restore to sea surface temperatures (SSTs). Instead, turbulent heat fluxes are derived from the NCAR

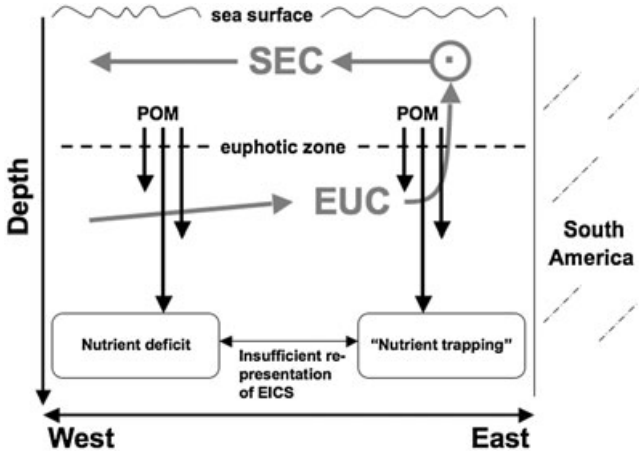

Figure 17. Schematic of "nutrient trapping" in the tropical eastern Pacific. The eastward EUC transports nutrients into the "nutrient trapping region" in the East. The core of the EUC is relatively deep in the West, approaches the euphotic zone as it travels East, and supplies the upwelling that crosses the euphotic zone in the "nutrient trapping region." This fuels biotic uptake of nutrients (primary production), a fraction of which is exported vertically by sinking particles (POM). The remainder is flushed out of the region (either still in inorganic form or bound in organic matter) by southward and westward (South Equatorial Current) surface currents. The sinking POM is remineralized at depth. This causes spuriously enhanced nutrient concentrations and an associated oxygen deficit in the east. In our simulations, we find an apparently associated problem, a "nutrient deficit" at depth in the west. We speculate that both problems are caused by a deficient simulation of the Equatorial Intermediate Current System and Equatorial Deep Jets.

bulk formulae using the simulated SST and the 10 m atmospheric fields. Salinity is restored toward the monthly mean World Ocean Atlas 2001 [*Boyer et al.*, 2002] with a time scale of 2 months. A freshwater flux is evenly distributed over the global surface ocean compensating for net water fluxes due to the combined effect of precipitation, evaporation, and river runoff such that the volume of the model ocean is conserved.

A1.2. ERA-40

[65] The configuration EDDY, set up from scratch, is driven by (six-hourly) wind stress, heat, and freshwater flux fields derived from the ERA-40 reanalyses from the European Centre for Medium-Range Weather Forecasts [*Uppala et al*., 2005, and many more to follow]. In addition to the heat fluxes from the ERA-40 reanalyses, a flux correction restores SST with a time scale of 30 days to monthly mean SST derived from a blend of satellite products (C. Rathbone, 2006, personal communication). Sea surface salinity is restored to the World Ocean Atlas 2001 [*Boyer et al.*, 2002] annual mean climatology with a time scale of 90 days. The vertical mixing of momentum and scalars is parameterized with the KPP approach of *Large et al.* [1994]. The relevant parameters are (1) a critical bulk Richardson number of 0.3 and (2) a vertical background diffusivity and viscosity of $10^{-5}\,m^2\,s^{-1}$. We account for double-diffusive and non-local fluxes. In all other respects, not described here, the configuration EDDY is identical to the configuration without data assimilation described by *Oke et al.* [2005] and used, e.g., by *Dietze et al.* [2009]. It is furthermore, except for the spacial grid, identical to the configurations used in *Liu et al.* [2010] and *Dietze and Kriest* [2012].

A2. Biogeochemical Models

[66] This study focuses on simulating global nutrient (and oxygen) concentrations. To first order, and as far as nutrients are concerned, all biogeochemical models can be understood simply as machineries which redistribute nutrients reaching the sunlit surface into two pools. One pool is redistributed to depth mimicking the effect of sinking particles while the other pool does not sink immediately but remains subject to relatively strong horizontal transport processes near the surface—until, after a time lag which is the intrinsic property of a biogeochemical model, it ultimately becomes also subject to sinking. In general, this time lag which decouples local photosynthetic production (or nutrient uptake) from local export production is not constant but a function of light, nutrients, temperature as well as of the past and present state of the model system. The formulations which result in the respective time lag can be arbitrarily complex. Hence, it is impossible to test all plausible formulations. However, we feel that the equations presented in the following are well suited to explore the plausible range of the decoupling between local nutrient uptake and local export production.

[67] All biogeochemical model simulations presented in this study are based on a so-called nutrient-phytoplankton-zooplankton-detritus (N-P-Z-D) formulation and are very similar to the one described by *Oschlies and Garçon* [1999]. This is a state-of-the-art approach as recent publications reveal [e.g., *Schmittner et al*., 2005; *Keller et al*., 2012], although realizations come in differing grades of complexity. Conceptional differences to *Oschlies and Garçon* [1999] applied in this study include the switch from nitrogen to phosphorous as the "base currency" of the model and the explicit simulation of dissolved organic phosphorous dynamics.

[68] The initial concentrations of phosphate, oxygen, and phytoplankton (assuming a Chl*a* to phosphorous ratio of $0.099\,mol\,P\,(g\,Chl\,a)^{-1}$) are annual means from the World Ocean Atlas 2001 [*Conkright et al.*, 2002a; *Locarnini et al.*, 2002; *Conkright et al.*, 2002b] interpolated onto respective model grids. Detritus and zooplankton were initialized with values corresponding to 1% of the initial phytoplankton concentration.

[69] The prognostic variables are nutrient phosphate (N), phytoplankton (P), zooplankton (Z), particulate detritus (D), and dissolved oxygen (O_2). In addition, some simulations feature dissolved organic phosphorous (DOP). Each prognostic variable C is determined following:

$$\frac{\partial C}{\partial t} = T + sms, \tag{A1}$$

where T denotes the spacial divergence of diffusive and advective transports. *sms* refers to the sources-minus-sinks term, which describe the biogeochemical interactions as follows:

[70] Phytoplankton (P) equation:

$$\text{sms (P)} = \overline{J}\text{P} - G\,(\text{P})\,\text{Z} - \mu_{\text{P}}\text{P}. \tag{A2}$$

[71] Zooplankton (Z) equation:

$$\text{sms (Z)} = \gamma_1 G\,(\text{P})\,\text{Z} - \gamma_2\text{Z} - \mu_{\text{Z}}\text{Z}^2. \tag{A3}$$

[72] Detritus (D) equation:

$$\text{sms (D)} = (1-\gamma_1)G\,(\text{P})\,\text{Z} + \mu_{\text{P}}\text{P} + \mu_{\text{Z}}\text{Z}^2 - \mu_{\text{D}}\text{D} - \mu_{\text{D2}}\text{D} - w_s\frac{\partial \text{D}}{\partial z}. \tag{A4}$$

[73] Phosphate nutrient (N) equation:

$$\text{sms (N)} = \mu_{\text{D}}\text{D} + \mu_{\text{DOP}}\text{DOP} + \gamma_2\text{Z} - \overline{J}\text{P}. \tag{A5}$$

In the absence of oxygen, we set μ_{D}, μ_{DOP}, and γ_2 to 0. Hence, instead of denitrification, the model features a spurious accumulation of detritus at the ocean's bottom.

[74] Dissolved organic phosphorous (DOP) equation:

$$\text{sms (DOP)} = \mu_{\text{D2}}\text{D} - \mu_{\text{DOP}}\text{DOP}. \tag{A6}$$

[75] Oxygen (O_2) equation:

$$\text{sms } (\text{O}_2) = F_{\text{sfc}} - \text{sms (N)}R_{\text{O}_2:\text{P}}. \tag{A7}$$

[76] Parameters and their values in the reference simulation (REF) are listed in Table 2. All parameter values changed in the other simulations are explained in Table 3.

A2.1. Phytoplankton Growth

[77] The function $\overline{J} = \overline{J}\,(I, \text{N})$ describes the growth rate of phytoplankton as a function of irradiance (I) and nutrient concentrations N (note that N refers to PO_4 in this study).

$$\overline{J}\,(I, \text{N}) = \min\,(J_I, J_{\max} u_{\text{PO}_4}). \tag{A8}$$

The maximum growth rate $J_{\max}$ is a function of temperature (T):

$$J_{\max}\,(\text{T}) = a \cdot \exp\left(\frac{\text{T}}{T_b}\right). \tag{A9}$$

The light-limited growth rate J_I is

$$J_I = \frac{J_{\max}\alpha I}{\left[J_{\max}^2 + (\alpha I)^2\right]^{1/2}}, \tag{A10}$$

where α is the initial slope of the photosynthesis versus irradiance (*P-I*) curve. The calculation of the photosynthetically active shortwave radiation I and the method of averaging the light-limited growth over 1 day is taken from *Evans and Parslow* [1985] and outlined in *Oschlies and Garçon* [1999] and *Schmittner et al.* [2005]. Nutrient limitation is represented by the product of $J_{\max}$ and the nutrient uptake rates $u_{\text{NO}_3} = \text{NO}_3/\,(k_{\text{NO}_3} + \text{NO}_3)$ and $u_{\text{PO}_4} = \text{PO}_4/\,(k_{\text{PO}_4} + \text{PO}_4)$, with $k_{\text{PO}_4} = k_{\text{NO}_3} R_{\text{PO}_4:\text{NO}_3}$ providing the respective nutrient uptake rates.

A2.2. Grazing

[78] Zooplankton grazing of phytoplankton G (P) is parameterized with a Holling-type-III function:

$$G\,(\text{P}) = \frac{g\epsilon\text{P}^2}{g + \epsilon\text{P}^2}. \tag{A11}$$

A2.3. Sinking of Detritus

[79] The rate of sinking of Detritus w_s is a linear function of depth z but cannot exceed a maximum value of w_{Dmax}:

$$w_s = w_s\,(z) = \min\,(w_{\text{D}_0} + m_w z, w_{\text{Dmax}}). \tag{A12}$$

Note that some simulations presented here were run with $m_w = 0$, i.e., with constant sinking speed.

A2.4. Air-Sea Gas Exchange

[80] Air-sea exchange of oxygen is parameterized following the OCMIP-2 protocol (R. G. Najjar and J. C. Orr, Design of OCMIP-2 simulations of chlorofluorocarbons, the solubility pump and common biogeochemistry, 1998; available from the World Wide Web at http://www.ipsl.jussieu.fr/OCMIP):

$$F_{\text{sfc}} = KW\left(O_2^{\text{surf}} - O_2^{\text{sat}}\right), \tag{A13}$$

where O_2^{surf} is the surface O_2 concentration computed by the model and

$$O_2^{\text{sat}} = O_2^{\text{sato}}\frac{P}{P_0}, \tag{A14}$$

where P is the (local) total air pressure at sea level and P_0 is 1 atm. O_2^{sato} is the oxygen saturation concentration at one atmosphere total pressure for water-saturated air calculated from simulated sea surface temperature and salinity following *Garcia and Gordon* [1992] (note that the $a_3 \cdot ts^2$ term in the paper is incorrect, it should not be there). KW is the piston velocity, calculated according to *Wanninkhof* [1992]:

$$KW = (1 - F_{\text{ice}})a\left(u^2 + v\right)(Sc\text{O}_2/660)^{-1/2}. \tag{A15}$$

with coefficient $a = 0.337\ \text{cm s}^2\ \text{h}^{-1}\ \text{m}^{-2}$ (which was tuned—original value proposed by *Wanninkhof* [1992] was 0.31—by the OCMIP group so that their global mean air-sea CO_2 exchange matches the *Broecker et al.* [1986] radiocarbon-calibrated estimate of $0.061\ \text{mol C m}^{-2}\ \text{a}^{-1}\ \mu\text{atm}^{-1}$) and the Schmidt number of oxygen in seawater $Sc\text{O}_2$ as a function of temperature as proposed by *Keeling et al.* [1998]. The square of monthly mean wind speed u^2 and the variance v of wind speed computed over 1 month as well as ice cover F_{ice} and sea level pressure were adopted from OCMIP2 and interpolated onto the model grid.

Appendix B: Transit Times

[81] Based on a mean meridional velocity of $0.1\ \text{m s}^{-1}$ which is rarely exceeded offshore, it takes ≈2 months for a water parcel to travel out of the equatorial upwelling 5° of latitude poleward. Assuming that a horizontal diffusivity of $1000\ \text{m}^2\text{s}^{-1}$ is an admissible representation of mixing induced by eddies, implies a diffusive transport time estimate of ≈8 years.

Appendix C: Error Estimates

[82] As already mentioned in the introduction, the region of interest features especially tight coupling between the ocean and the atmosphere. This, in turn, results in both a high temporal variability and high uncertainties of observational estimates in general. The latter holds also for the EUC transport and the upwelling where, to cite *Kessler* [2006],

"we know, as Wyrtki did, that some of the EUC upwells into the SEC, while another part continues southward at thermocline depth to feed the Peru upwelling but are not much further along in putting numbers to this than was possible 1966." In the following, our error estimates denoted by red patches in Figure 11 are explained:

[83] 1. The upper and lower bounds of regionally (see Figure 1) averaged sea surface temperature are based on "objectively analyzed" works of *Locarnini et al.* [2010] and *Reynolds et al.* [2002], respectively. This range comprises both a 2002–2005 average based on MODIS level 3 data [*Savtchenko et al.*, 2004] and the "statistical mean" climatology of *Locarnini et al.* [2010].

[84] 2. The monthly mean heat flux estimates are highly uncertain (NOCS Surface Flux Dataset v2.0) [*Berry and Kent*, 2011, Figure 2]. Averaging over longer periods should reduce the error, given that the errors are independent from one another. Because we do not know if this holds, we plotted the standard deviation of annual means which is, admittedly, an estimate of interannual variability rather than an error estimate.

[85] 3. The EUC transport estimates entering the "nutrient trapping region" at 130°W (20–40 Sv) are derived from *Johnson et al.* [2002, their Figure 17] who found 20–33 Sv at 140°W and 27–40 Sv at 125°W.

[86] 4. The upwelling is between 30 and 50 Sv according to *Kessler* [2006, and references therein].

[87] **Acknowledgments.** Discussions with W. Köve, P. Brandt, and K. Böning and long-term support by A. Oschlies are appreciated. Integrations were performed on a NEC-SX9 at the University Kiel, Germany, and on scalar architectures at GEOMAR. This study was supported by the German DFG as part of the SFB 754.

References

Abell, J., S. Emerson, and P. Renaud (2000), Distributions of TOP, TON and TOC in the North Pacific subtropical gyre: Implications for nutrient supply in the surface ocean and remineralization in the upper thermocline, *J. Mar. Res*, *58*(2), 203–222 , doi:10.1357/002224000321511142.

Anderson, L., and J. Sarmiento (1995), Global ocean phosphate and oxygen simulations, *Global Biogeochem. Cy.*, *9*(4), 621–636.

Antonov, J. I., D. Seidov, T. P. Boyer, R. A. Locarnini, A. V. Mishonov, H. E. Garcia, O. K. Baranova, M. M. Zweng, and D. R. Johnson (2010), *World Ocean Atlas 2009, Volume 2: Salinity*. NOAA Atlas NESDIS 69.

Ascani, F., E. Firing, P. Dutrieux, J. P. McCreary, and A. Ishida (2010), Deep equatorial ocean circulation induced by a forced-dissipated Yanai beam, *J. Phys. Oceanogr.*, *40*(5), 1118–1142 , doi: 10.1175/2010JPO4356.1.

Aumont, O., J. Orr, P. Monfray, G. Madec, and E. Maier-Reimer (1999), Nutrient trapping in the equatorial Pacific: The ocean circulation solution, *Global Biogeochem. Cy.*, *13*(2), 351–369.

Behrenfeld, M. J., and P. G. Falkowski (1997), Photosynthetic rates derived from satellite-based chlorophyll concentration, *Limnol. Oceanogr.*, *42*(1), 1–20.

Berry, D., and E. Kent (2011), Air-sea fluxes from ICOADS: The construction of a new gridded dataset with uncertainty estimates, *Int. J. Climatol.*, *31*, 987–1001, doi:10.1002/joc.2059.

Boyer, T. P., C. Stephens, J. I. Antonov, M. E. Conkright, R. A. Locarnini, T. D. O'Brian, and H. E. Garcia (2002), *World Ocean Atlas 2001, Volume 2: Salinity*. NOAA Atlas NESDIS 50, 167 pp., CD-ROMs.

Broecker, W. S., J. R. Ledwell, T. Takahashi, R. Weiss, L. Merlivat, L. Memery, T.-H. Peng, B. Jahne, and K. O. Munnich (1986), Isotopic versus micrometeorologic ocean CO_2 fluxes, *J. Geophys. Res.-Oceans*, *91*(C9), 10517–10527.

Conkright, M. E., H. E. Garcia, T. D. O'Brian, R. A. Locarnini, T. P. Boyer, C. Stephens, and J. I. Antonov (2002a), *World Ocean Atlas 2001, Volume 4: Nutrients*. NOAA Atlas NESDIS 52, 392 pp., CD-ROMs.

Conkright, M. E., T. D. O'Brian, C. Stephens, R. A. Locarnini, H. E. Garcia, T. P. Boyer, and J. I. Antonov (2002b), *World Ocean Atlas 2001, Volume 6: Chlorophyll*. NOAA Atlas NESDIS 52, 46 pp., CD-ROMs.

Cravatte, S., W. Kessler, and F. Marin (2012), Intermediate zonal jets in the tropical Pacific Ocean observed by Argo floats, *J. Phys. Oceanogr.*, *42*(9), 1475–1485, doi:10.1175/JPO-D-11-0206.1.

Dietze, H., and I. Kriest (2012), ^{137}Cs off Fukushima Dai-ichi, Japan—Model based estimates of dilution and fate, *Ocean Sci.*, *8*(3), 319–332, doi:10.5194/os-8-319-2012.

Dietze, H., R. J. Matear, and T. S. Moore (2009), Nutrient supply to anticyclonic meso-scale eddies off Western Australia estimated with artificial tracers released in a circulation model, *Deep-Sea Res. Pt. I*, *56*(9), 1440–1448, doi:10.1016/j.dsr.2009.04.012.

Duteil, O., et al. (2012), Preformed and regenerated phosphate in ocean general circulation models: Can right total concentrations be wrong? *Biogeosciences*, *9*, 1797–1807, doi: 10.5194/bg-9-1797-2012.

Evans, G. T., and J. S. Parslow (1985), A model of annual plankton cycles, *Biol. Oceanogr.*, *3*, 328–347.

Garcia, H. E., and L. I. Gordon (1992), Oxygen solubility in seawater: Better fitting equations, *Limnol. Oceanogr.*, *37*(6), 1307–1312.

Garcia, H. E., R. A. Locarnini, T. P. Boyer, J. I. Antonov, O. K. Baranova, M. M. Zweng, and D. R. Johnson (2010a), *World Ocean Atlas 2009, Volume 3: Dissolved oxygen, apparent oxygen utilization, and oxygen saturation*, NOAA Atlas NESDIS 70.

Garcia, H. E., R. A. Locarnini, T. P. Boyer, J. I. Antonov, M. M. Zweng, O. K. Baranova, and D. R. Johnson (2010b), *World Ocean Atlas 2009, Volume 4: Nutrients (phosphate, nitrate, silicate)*, NOAA Atlas NESDIS 71.

Gnanadesikan, A., et al. (2006), GFDL's CM2 global coupled climate models. Part II: The baseline ocean simulation, *J. Climate*, *19*(5), 675–697, 76, doi:10.1175/JCLI3630.1.

Griffies, A. M., A. W. D. K. Gnanadesikan, J. P. Dunne, R. Gerdes, M. J. Harrison, A. Rosati, J. L. Russell, B. L. Samuels, M. J. Spelman, and M. R. Z. Winton (2005), Formulation of an ocean model for global climate simulations, *Ocean Sci.*, *1*, 45–79, doi:10.5194/os-1-45-2005.

Hundsdorfer, W., and R. Trompert (1994), Method of lines and direct discritisation: A comparison for linear advection, *Appl. Numer. Math., 13*, 469–490.

Johnson, G., B. Sloyan, W. S. Kessler, and K. McTaggart (2002), Direct measurements of upper ocean currents and water properties across the tropical Pacific during the 1990s, *Prog. Oceanogr.*, *52*(1), 31–61, doi:10.1016/S0079-6611(02)00021-6.

Karl, D. M., and K. M. Björkman (2002), *Dynamics of DOP*, in *Biogeochemistry of Marine Dissolved Organic Matter*, edited by D.A. Hansell, and C. A. Carlson, p. 246–366. , Academic Press, San Diego.

Karstensen, J., L. Stramma, and M. Visbeck (2008), Oxygen minimum zones in the eastern tropical Atlantic and Pacific Oceans, *Prog. Oceanogr.*, *77*(4), 331–350, doi:10.1016/j.pocean.2007.05.009.

Keeling, R. F., B. B. Stephens, R. G. Najjar, S. C. Doney, D. Archer, and M. Heimann (1998), Seasonal variations in the atmospheric O_2/N_2 ratio in relation to the kinetics of air-sea gas exchange, *Global Biogeochem. Cy.*, *12*, 141–163.

Keller, D. P., A. Oschlies, and M. Eby (2012), A new marine ecosystem model for the University of Victoria Earth System Climate Model, *Geosci. Model Dev.*, *5*, 1195–1220, doi:10.5194/gmd-5-1195-2012.

Kessler, W. S. (2006), The circulation of the eastern tropical Pacific: A review, *Prog. Oceanogr.*, *69*(2-4), 181–217, doi:10.1016/j.pocean.2006.03.009.

Kwon, E. Y., and F. Primeau (2006), Optimization and sensitivity study of a biogeochemistry ocean model using an implicit solver and in situ phosphate data, *Global Biogeochem. Cycles*, *20, GB4009*, doi: 10.1029/2005GB002631.

Large, W., and S. Yeager, (2004), Diurnal to decadal global forcing for ocean and sea-ice models: The data sets and flux climatologies, *NCAR Technical Note: NCAR/TN-460+STR*.

Large, W. G., J. C. McWilliams, and S. C. Doney (1994), Oceanic vertical mixing—A review and a model with a nonlocal boundary-layer parameterization, *Rev. Geophys.*, *32*(4), 363–403.

Lebedev, K. V., H. Yoshinari, N. A. Maximenko, and P. W. Hacker, (2007), YoMaHa'07: Velocity data assessed from trajectories of Argo floats at parking level and at the sea surface, *IPRC Technical Note 4 (2)*.

Liu, N., C. Eden, H. Dietze, D. Wu, and X. Lin (2010), Model-based estimate of the heat budget in the East China Sea, *J. Geophys. Res.-Oceans*, *115, C08026*, doi: 10.1029/2009JC005869.

Locarnini, R. A., A. V. Mishonov, J. I. Antonov, T. P. Boyer, H. E. Garcia, O. K. Baranova, M. M. Zweng, and D. R. Johnson (2010), *World Ocean Atlas 2009, Volume 1: Temperature*, NOAA Atlas NESDIS 68.

Locarnini, R. A., T. D. O'Brian, H. E. Garcia, J. I. Antonov, T. P. Boyer, M. E. Conkright, and C. Stephens (2002), *World Ocean Atlas 2001, Volume 3: Oxygen*. NOAA Atlas NESDIS 51, 286 pp., CD-ROMs.

Loeptien, U., C. Eden, A. Timmermann, and H. Dietze (2009), Effects of biologically induced differential heating in an eddy-permitting coupled

ocean-ecosystem model, *J. Geophys. Res.-Oceans*, *114, C06011*, doi: 10.1029/2008JC004936.

Maier-Reimer, E. (1993), Geochemical cycles in an ocean general circulation model. Preindustrial tracer distributions, *Global Biogeochem. Cycles*, *7*(3), 645–677.

Matear, R., and G. Holloway (1995), Modeling the inorganic phosphorus cycle of the north Pacific using an adjoint data assimilation model to assess the role of dissolved organic phosphorus, *Global Biogeochem. Cycles*, *9*(1), 101–119.

Najjar, R., J. Sarmiento, and J. Toggweiler (1992), Downward transport and fate of organic matter in the ocean: Simulations with a general circulation model, *Global Biogeochem. Cycles*, *6*(1), 45–76.

Oke, P. R., A. Schiller, D. A. Griffin, and G. B. Brassington (2005), Ensemble data assimilation for an eddy-resolving ocean model of the Australian region, *Q. J. Roy. Meteor. Soc.*, *131*, 3301–3311, doi:10.1256/qj.05.95.

Oschlies, A. (2000), Equatorial nutrient trapping in biogeochemical ocean models: The role of advection numerics, *Global Biogeochem. Cycles*, *14*, 655–667, doi:10.1029/1999GB001217.

Oschlies, A., and V. Garçon (1999), An eddy-permitting coupled physical-biological model of the North Atlantic. Part I: Sensitivity to advection numerics and mixed layer physics, *Global Biogeochem. Cycles*, *13*, 135–160, doi:10.1029/98GB02811.

Rafter, P. A., D. M. Sigman, C. D. Charles, J. Kaiser, and G. H. Haug (2012), Subsurface tropical Pacific nitrogen isotopic composition of nitrate: Biogeochemical signals and their transport, *Global Biogeochem. Cycles*, *26*, GB1003, doi:10.1029/2010GB003979.

Reynolds, R., N. Rayner, T. Smith, D. Stokes, and W. Wang (2002), An improved in situ and satellite SST analysis for climate, *J. Climate*, *15*(13), 1609–1625, doi:10.1175/1520-0442(2002)015 <1609:AIISAS>2.0.CO;2.

Savtchenko, A., D. Ouzounov, S. Ahmad, J. Acker, G. Leptoukh, J. Koziana, and D. Nickless (2004), Terra and Aqua Modis products available from NASA GES DAAC, *Adv. Space Res.*, *34*(4), 710–714, doi: 10.1016/j.asr.2004.03.012.

Schmittner, A., A. Oschlies, X. Giraud, M. Eby, and H. L. Simmons (2005), A global model of the marine ecosystem for long term simulations:Sensitivity to ocean mixing, buoyancy forcing, particle sinking and dissolved organic matter cycling, *Global Biogeochem. Cycles*, *19, GB3004*, doi:10.1029/2004GB002283.

Schmittner, A., A. Oschlies, H. D. Matthews, and E. D. Galbraith (2008), Future changes in climate, ocean circulation, ecosystems, and biogeochemical cycling simulated for a business-as-usual CO_2 emission scenario until year 4000 AD, *Global Biogeochem. Cycles*, *22, GB1013*, doi:10.1029/2007GB002953.

Sweby, P. (1984), High-resolution schemes using flux limiters for hyperbolic conservation-laws, *SIAM J. Numer. Anal.*, *21*, 995–1011.

Uppala, S. M., et al. (2005), The ERA-40 re-analysis, *Q. J. Roy. Meteor. Soc.*, *131*(612), 2961–3012, doi:10.1256/qj.04.176.

Wanninkhof, R. (1992), Relationship between wind speed and gas exchange over the ocean, *J. Geophys. Res._Oceans*, *97*, 7373–7382.

Weaver, A. J., et al. (2001), The UVic earth system climate model: Model description, climatology, and applications to past, present and future climates, *Atmos. Ocean*, *39* (4), 361–428, doi: 10.1080/07055900.2001.9649686.

Wyrtki, K. (1981), An estimate of equatorial upwelling in the Pacific, *J. Phys. Oceanogr.*, *11*, 1205–1214.

Yoshimura, T., J. Nishioka, H. Saito, S. Takeda, A. Tsuda, and M. L. Wells (2007), Distributions of particulate and dissolved organic and inorganic phosphorus in north Pacific surface waters, *Mar. Chem.*, *103*(1-2), 112–121, doi:10.1016/j.marchem.2006.06.011.

Zamora, L. M., A. Landolfi, A. Oschlies, D. A. Hansell, H. Dietze, and F. Dentener (2010), Atmospheric deposition of nutrients and excess N formation in the North Atlantic, *Biogeosciences*, *7*, 777–793, doi:10.5194/bg-7-777-2010.

Zhang, X., and M. J. McPhaden (2010), Surface layer heat balance in the eastern equatorial Pacific ocean on interannual time scales: Influence of local versus remote wind forcing, *J. Climate*, *23*(16), 4375–4394, doi: 10.1175/2010JCLI3469.1.